

A Project Report On

Electric-Drive-Reconstructed Onboard Charger for Solar-Powered Electric Vehicles Incorporating Six-Phase Machine

Submitted to

JAWAHARLAL NEHRU TECHNOLOGICAL UNIVERSITY, ANANTHAPURAMU

In Partial Fulfillment of the Requirements for the Award of the Degree of

**BACHELOR OF TECHNOLOGY
IN
ELECTRICAL AND ELECTRONICS ENGINEERING**

Submitted by

GUDIMETLA SNEHANJALI	219E1A0222
MALLA YASHWANTHI	219E1A0242
E DURGASRI	219E1A0217
MEKALA SNEHA LATHA	219E1A0245
KODIKANTI GREESHMA	219E1A0231

Under the esteemed guidance of

Mrs. K. PRATHIBHA, M.Tech.(Ph.D)

ASSISTANT PROFESSOR



DEPARTMENT OF ELECTRICAL AND ELECTRONICS ENGINEERING

SRI VENKATESWARA ENGINEERING COLLEGE

(Approved by AICTE, New Delhi, NBA & NAAC Accredited Institution with UGC section 2(f) & 12(b) & Affiliated to JNTUA, Anantapuramu)

**Karakambadi Road, Tirupati - 517507
(2021-2025)**

SRI VENKATESWARA ENGINEERING COLLEGE
DEPARTMENT OF ELECTRICAL AND ELECTRONICS ENGINEERING
(Accredited by NBA & NAAC)
UGC section 2(f) & 12(B) Approved by AICTE, New Delhi & Affiliated to JNTUA,
Ananthapuramu
Karakambadi Road, Tirupati- 517507



CERTIFICATE

This is to certify that the Project report entitled

“Electric-Drive-Reconstructed Onboard Charger for Solar-Powered Electric Vehicles Incorporating Six-Phase Machine”

is the bonafide work carried out by

GUDIMETLA SNEHANJALI	219E1A0222
MALLA YASHWANTHI	219E1A0242
E DURGASRI	219E1A0217
MEKALA SNEHA LATHA	219E1A0245
KODIKANTI GREESHMA	219E1A0231

Towards the partial fulfilment of the requirements for the award of the degree of
BACHELOR OF TECHNOLOGY in **ELECTRICAL & ELECTRONICS**
ENGINEERING from JNTUA, Ananthapuramu during the year 2021 - 2025

GUIDE:

Mr. K. PRATHIBHA, M. Tech, (Ph. D.) Assistant Professor
Dept. of EEE

HEAD OF THE DEPARTMENT:

Dr. SHAIK RAFI KIRAN, M.Tech., Ph.D. Professor & HOD
Dept. of EEE

Viva – Voice held on _____

INTERNAL EXAMINER

i

EXTERNAL EXAMINER

ACKNOWLEDGEMENT

We are sincerely thankful to our guide **Mr. K. PRATHIBHA, M. Tech. (Ph.D.),, Assistant Professor**, for her valuable guidance and encouragement. Her helping attitude and suggestions have helped in the successful completion of the project report.

We would like to express our gratefulness and sincere thanks to **Dr. SHAIK RAFI KIRAN, Professor & Head, Department of EEE**, for his kind help and encouragement during the course of study and in the successful completion of the project report.

We would like to express our heartfelt thanks to **Dr. C. CHANDRASEKHAR, Principal**, for successful completion of this project report, which cannot be done without proper support and encouragement.

We sincerely thank the **Management** for providing all the necessary facilities during the course of study.

We would like to express our deep gratitude to all those who helped directly or indirectly to transform an idea into our working project report, necessary facilities during the course of study.

GUDIMETLA SNEHANJALI **219E1A0222**

MALLA YASHWANTHI **219E1A0242**

E DURGASRI **219E1A0217**

MEKALA SNEHA LATHA **219E1A0245**

KODIKANTI GREESHMA **219E1A0231**

ABSTRACT

In this project, a novel electric-drive-reconstructed onboard charger (EDROC) is proposed for the solar-powered electric vehicle that incorporates a six-phase machine drive. The power traction inverter and the machine are re-leveraged to implement charging operation, further minimizing the incremental mass accordingly. In particular, charging and driving operations can be simultaneously carried out via the vehicle-roof photovoltaic panels, significantly expanding EV mileage range. First, the operation scenario and the topology of the proposed EDROC are introduced. Next, the operational principle is analyzed, as well as the indispensable conditions for safe and stable operation are studied. Thereafter, control schemes are designed and elaborated in terms of the simultaneous driving and charging mode and the dc charging mode. the proposed method simulation results are presented to verify the steady-state and dynamic behavior of the proposed EDROC system under different operation modes.

Keywords: Electric-drive-reconstructed onboard charger (EDROC), simultaneous driving and charging, six-phase machine, solar-powered electric vehicle (EV), vehicle-roof photovoltaic panels (PPs).

DECLARATION

We hereby declare that the project entitled "**Electric-Drive-Reconstructed Onboard Charger for Solar-Powered Electric Vehicles Incorporating Six-Phase Machine**", submitted to the Department of Electrical and Electronics Engineering at **S.V. Engineering College, Tirupati**, in partial fulfillment of requirements for the award of the degree of **Bachelor of Technology in Electrical and Electronics Engineering**.

This report is the result of our own effort and it has not been submitted to any other University or Institution for the award of any degree or diploma other than specified above.

GUDIMETLA SNEHANJALI

219E1A0222

MALLA YASHWANTHI

219E1A0242

E DURGASRI

219E1A0217

MEKALA SNEHA LATHA

219E1A0245

KODIKANTI GREESHMA

219E1A0231

CONTENTS

CERTIFICATE	i	
ACKNOWLEDGEMENT	i	
ABSTRACT	ii	
DECLARATION	iv	
CONTENTS	v-vi	
LIST OF FIGURES	vii-viii	
LIST OF TABLES	ix	
CHAPTER 1	INTRODUCTION	01-08
	1.1 Introduction	01
	1.2 Literature survey	04
	1.3 Existing method	06
	1.3.1 Disadvantages	07
	1.4 Proposed system	07
	1.4.1 System configuration	07
	1.4.2 Advantages	07
	1.5 Applications	07
	1.6 Objective of the project	07
	1.7 Organization of the project	08
CHAPTER 2	SOLAR PV AND BATTERY	09-17
	2.1 Introduction	09-12
	2.2 Efficiency	11-12
	2.2.1 Applications	12
	2.2.2 Advantages	13
	2.3 Battery	13
	2.3.1 Lithium-ion battery	14-15
	2.3.2 History	16-17
CHAPTER 3	DC-AC CONVERTER AND PMSM	18-25
	3.1 DC-AC converter	18
	3.1.1 Introduction to power electronics	18
	3.1.2 Voltage Sources Inverter	19
	3.1.3 Current Source Inverter	19-20
	3.2 Permanent Magnet Synchronous Motor	21
	3.2.1 Introduction to PMSM construction and working	21
	3.2.2 Machine Configurations/ Configurations	21-22
	3.2.3 Flux Density Distribution	23
	3.2.4 Line Start PMSM	23
	3.2.5 Various control Strategies of PMSM	23
	3.2.6 Model of PMSM motor	24-25
CHAPTER 4	ELECTRIC VEHICLES	26-32
	4.1 Introduction	26
	4.2 History	27-28

4.3 Experimentation	28	
4.4 Reintroduction	29	
4.5 Electricity Sources	29	
4.5.1 Connections to Generator Plants	30	
4.5.2 On Board Generator and Hybrid EV	30-32	
CHAPTER 5	TOPOLOGY OF PROPOSED EDROC	33-44
5.1 Introduction	33	
5.2 DC Charging Mode	33-34	
5.3 Simultaneous Driving and Chargin Mode	34	
5.4 Operation Principle of EDROC	35	
5.4.1 DC Charging Mode	36	
5.4.1.1 Building the Model	36-38	
5.4.2 Simultaneous Charging and Driving	38-40	
5.5 Necessary Conditions for EDROC	40-42	
5.6 Magnetizing Signals and Parameters	42	
5.6.1 MPPT and Constant Voltage/Current Charging	42-43	
Control		
5.6.1.1 DC Charging Mode	43	
5.6.1.2 Simultaneous Charging and Driving Mode	44	
CHAPTER 6	SIMULATION RESULTS	45-61
6.1 Case-1-DC Charging Mode	45-46	
6.1.1 Controlling Unit	46	
6.1.2 Reference Current	47	
6.1.3 Source Code [Parameters]	48	
6.1.3.1 Mode-0	49-50	
6.1.3.2 Mode-1	51-52	
6.2 Case-2 – Simultaneous Charging and Driving Mode	52	
6.2.1 Load and Speed Constant	53	
6.2.2 Controlling unit	54	
6.2.3 Speed Control Unit	54	
6.2.4 Source Code [Dynamic load]	55	
6.2.4.1 Both Load and Speed	56-58	
are Constant		
6.2.4.2 Load Variable and		
Speed Constant	59	
6.2.4.3 Load Constant and		
Speed Variable	60	
6.3 Results analysis	61	
CONCLUSION & FUTURE SCOPE	62	
REFERENCES	63-64	

LIST OF FIGURES

Fig. No.	DESCRIPTION	PAGE
		No.
1.1	On board charger V/S off board charger	01
2.1	Solar PV array	09
2.2	Array flow diagram	11
2.3	DC grid system	14
2.4	Battery (Rechargeable)	15
2.5	Battery mode	17
3.1	Voltage-source inverter	19
3.2	Current-source inverter	20
3.3	Surface PM(SPM) Synchronous motor	22
3.4	Model of PMSM	24
4.1	Passenger train, taking power through a third rail with return through the traction rails	29
4.2	An electric locomotive at Brig, Switzerland	30
4.3	The MAZ-7907 uses an on-board generator to power in-wheel electric motors	30
5.1	Proposed topology of six-phase EDROC	33
5.2(a)	Simplified system circuit in DC charging mode	34
5.2(b)	Equivalent circuits	34
5.3	Equivalent system circuit in simultaneous charging and driving mode	34
5.4	Further equivalent circuit operation states I, II, III, IV	35
5.5	Waveform of Idc and states of SXL and SYH	36
5.6	Winding arrangement of six phase PMSM	39
5.7	Equivalent systems structure in simultaneous driving and charging mode	39
5.8	Power distribution in simultaneous driving and charging mode	40
5.9	MPPT and constant voltage/current charging block diagram	42

6.1	Control diagram	45
6.2	Schematic diagram	46
6.3	Controlling part	46
6.4	Reference current	47
6.5	Steady state connected to grid	49
6.6	Dynamic state connected to solar	50
6.7	Steady state connected to grid	51
6.8	Dynamic state connected to solar	52
6.9	Schematic diagram	53
6.10	Controlling part	54
6.11	Speed controller	54
6.12	PPs output current and voltage, battery current and 01-axis current	56
6.13	Currents in d-axis, q-axis, x-axis and y-axis	57
6.14	Currents in phase A and U, speed and output torque (Both load and speed constant)	58
6.15	Currents in phase A and U, speed and output torque (Load variable and speed constant)	59
6.16	Currents in phase A and U, speed and output torque (Load constant and speed variable)	60

LIST OF TABLES

S. No.	NAME OF TABLE	PAGE No.
1.1	On-board storage	31

CHAPTER 1

INTRODUCTION

1.1 INTRODUCTION:

The popularity of electric vehicle (EV) is rising continuously due to its advantages over the one supplied by fossil fuels, mainly including zero emission, lower operational cost, higher efficiency, and lower noise. Thus, as one of the key technologies related to EV, charging technology has drawn considerable concern in the past decades. Traditionally, there are two types of chargers for EV available in market:

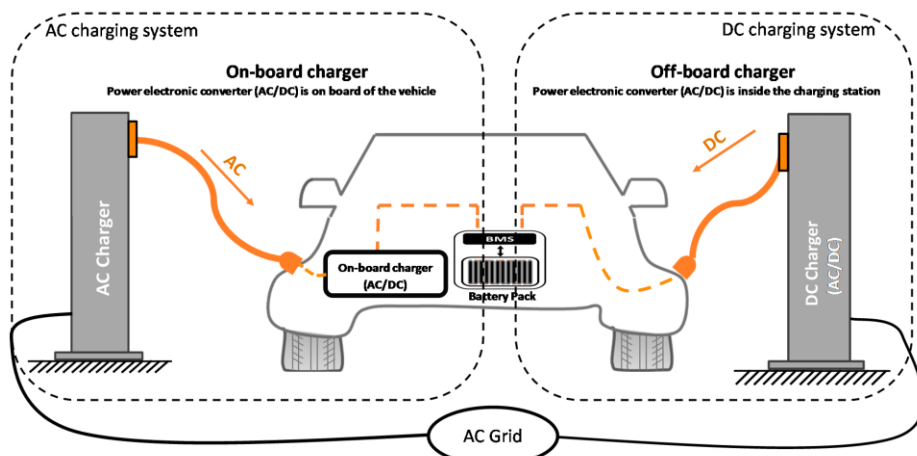


Fig.1.1. On-board charger & Off-board charger

off-board charger usually installed in fixed locations; and on-board independent charger mounted on EV. Even though off-board charger features the capacity of high-power fast charging, it currently encounters the issues of high cost and low geographic density. Comparatively, on-board independent charger appears to be more promising, not only for its acceptable price, but also for its ability to charge EV wherever there exists an electric power socket. However, from the EV perspective, on-board independent charger results in additional huge volume, weight as well as cost. As such, electric-drive-reconstructed onboard charger (EDROC) is proposed, where the existing drive system is reutilized for charging purpose, with the bulky components inherently exist in an on-board independent charger saved accordingly. Therefore, a lot of efforts have been put into the development of EDROC, and numerous topologies are studied. The EDROC topologies in tandem with three-phase drive have been introduced and successfully proven. Furthermore, an EDROC with the capability of active filter is studied to address pulsating power at twice of the line frequency exiting. And a split-windings machine is employed to construct an EDROC to bypass the issue of generating non-

negligible torque. Compared with three-phase machines, multi-phase machine drives have many significant advantages, such as the smooth torque generation and the distinct fault tolerance capacity. Therefore, multiphase machine drives have become serious contenders since 1990s not only in EV applications but also in other variable-speed applications, such as ship propulsion, locomotive traction, and aircraft. On the other hand, several enterprises have issued their multi-phase powertrain systems for EV, such as the SUMO series from DANA TM4. Based on multi-phase machine drives, a series of multi-phase EDROCs have been proposed successively. Referring to, two interesting EDROC topologies connecting to three-phase grid are investigated, incorporating asymmetrical and symmetrical six-phase machine drives, respectively. To improve grid voltage compatibility, an EDROC based on symmetrical nine-phase permanent magnet synchronous machine (PMSM) drive is developed, where the nine-phase drive system is reconstructed into two rectifiers connected in parallel along with a buck converter. Although the aforementioned multiphase EDROCs cleverly avoid the demerits of the traditional EV chargers and have been comprehensively studied, they are powered by electricity grid where the energy is currently derived from fossil fuels to a large extent. In other words, reducing the usage of fossil fuels and the emission are still unsatisfactory in terms of EVs purely supplied by electricity grid. As such, the EV fed by the renewable energy resources, such as solar energy is more and more attractive. In practice, solar-powered EV was researched by scholars and has been designed by car companies, such as Tesla, Audi, and Toyota. For instance, a solar-powered EV developed by NEDO, Sharp, and Toyota companies has been public tested from July 2019; the rated power generation of its vehicle-roof photovoltaic panels (PPs) is around 860 W, which is responsible for charging battery. Besides, Lightyear Company launched a solar-powered EV named Lightyear One, in 2019, and the power generated by its vehicle-roof PPs in an hour can extend 12 km of range in average. This results in a range increase of 60 km per day, if the battery is charged through the vehicle-roof PPs for an average of 5 h. Thus, if the average driving range per day is less than 60 km, it is possible to drive the vehicle for months without charging, which is almost for free and completely environmentally friendly. Dedicated to this type of EVs, an improved EDROC is proposed where the battery can be charged from emerging dc grid, utility storage or renewable energy resource. Meanwhile, a novel operation mode realizing simultaneous driving and charging is originally proposed, significantly extending the mileage range. However, an extra dc–dc converter is required to adjust charging current, which means additional cost. In addition, incorporating switched reluctance machine drive, an EDROC for solar-powered EV is studied. In this EDROC topology, in addition to two mode switching relays, no additional power devices are required. While in

simultaneous driving and charging mode, the vehicle-roof PPs and battery are directly connected in parallel. Thus, the output voltage of the vehicle-roof PPs must be roughly equal to the battery voltage and the maximum power point tracking (MPPT) for the vehicle-roof PPs fails to be implemented. In order to address these aforementioned issues, this article proposes a novel EDROC for solar-powered EV incorporating six-phase drive, in which supernumerary components are saved except for two mode switches as shown in Fig. 1.1 The developed EDROC has three main advantages. First, as long as the sunlight is strong enough, simultaneous driving and charging mode can operate by drawing power from the vehicle-roof PPs, expanding the mileage range of EV. Second, the EDROC can be supplied by renewable energy resources, such as emerging dc grid, utility storage, and vehicle-roof PPs, increasing the proportion of renewable energy with respect to the overall energy consumption.

Third, from the EV perspective, only two extra switches are added, and at the same time the existing six-phase drive system has no change in structure for all the operation modes, therefore the charger is cheaper, smaller and more reliable. Particularly, the proposed EDROC can be implemented in terms of both symmetrical and asymmetrical six-phase machines with a simple modification releasing the two available neutral points of the machine required. The major contributions of this article are listed as follows.

- 1) A novel EDROC topology incorporating a six-phase machine drive for the solar-powered EV is proposed, which integrates the PPs of the solar-powered EV into the topology without additional dc/dc converter. Although ac charging operation is not discussed, the proposed EDROC can be reconstructed as ac charger.
- 2) The vector control of six-phase machine is extended to the simultaneous driving and charging mode. Besides, necessary conditions for the EDROC in this mode are analyzed in detail to ensure EV safe operation.
- 3) An average duty strategy in conjunction with the phase shift technique is employed to implement the dc charging mode, highly suppressing the charging current ripple.

The vehicle-roof PPs and battery are directly connected in parallel. Thus, the output voltage of the vehicle-roof PPs must be roughly equal to the battery voltage and the maximum power point tracking (MPPT) for the vehicle-roof PPs fails to be implemented. In order to address these aforementioned issues, this article proposes a novel EDROC for solar-powered EV incorporating six-phase drive, in which supernumerary components are saved except for two mode switches.

1.2 LITERATURE SURVEY

[1] **Y. Zhang, J. Fang, F. Gao, S. Gao, D. Rogers, and X. Zhu**, proposes an isolated multifunctional charger topology is proposed. The charging system can be used to charge the auxiliary batteries or serve as an active filter (AF) for the power battery charger. By time-sharing multiplexing it, the high-frequency (HF) and low-frequency (LF/second harmonic) current ripple can be suppressed in driving and parking charging modes, respectively. The proposed topology can also achieve zero voltage switching for all power switches under a full-load range in the driving charging mode. In addition, the integration and the power density of the charging system can be improved due to the reconstruction of the capacitive energy storage AF in the parking charging mode. Finally, a 400-W experimental prototype is developed and the experimental results are presented to validate the performance and feasibility of the proposed topology.

[2] **D. Abeywardana, P. Acuna, and B. Hredzak**, proposes a way to provide V2G reactive power compensation through a boost inverter-based single stage EV charger and a DC-side capacitor without adversely affecting the EV battery. The operation of the boost inverter-based EV charger with second-order harmonic and switching frequency ripple current reduction, the dynamic behavior of the system, the transition between different operating modes, the DC-side capacitor voltage control above a minimum allowed voltage, and the DC-side capacitor sizing are extensively analyzed. The performance of the proposed system is verified using an experimental prototype, and presented results demonstrate the ability of the system to provide V2G reactive power compensation both with and without the EV battery.

[3] **R. Hou and A. Emadi**, proposes an obstacle for improving the power density as well as reducing the cost. This paper proposes a simple and effective method that reduces the bulk capacitor in single-phase chargers and alleviates the low-frequency sinusoidal harmonic current in automotive applications. It applies the low-voltage (LV) battery charger auxiliary power module as an AF to filter the low-frequency harmonic currents in the high-voltage (HV) battery charger when the HV battery is charging. Hence, the integrated active filter auxiliary power module (AFAPM)-based dual-voltage charging system can achieve the AF function without extra power switches, heat sinks, and corresponding gate-drive circuits. In addition, the proposed AFAPM converter can obtain an almost unchanged switch rating to achieve 2.4-kW LV battery charging and 6.6-kW HV active filtering functions. Therefore, the proposed method can reduce the cost for the dual-voltage charging system

in electrified vehicles. A 1.2-kW proof-of-concept prototype has also been built and experiments show promising results confirming the effectiveness of the proposed concept.

[4] **J. Gao, W. Sun, D. Jiang, Y. Zhang, and R. Qu**, proposes Single-phase grid-connected integrated on-board charger (IOBC) can significantly reduce the cost and the bulk of electric vehicles and has been used in real products. However, there are still two problems that have not been discussed and solved. First, when permanent magnet synchronous motor drives are used for single-phase IOBC, there are second-order current harmonic and the possibility of instability in the system. Second, when multiphase motor (MPM) drives are used for single-phase IOBC, the currents' assignment strategy and the dc voltage utilization of inverter need to be dissected. This article does detailed research work about these two problems. The origin of the second-order harmonic and the instability are exposed. Furthermore, proportional-double-resonant regulator and adaptive proportional (P) parameter control schemes are proposed to solve these problems. The operation principle of single-phase IOBC with MPM drive is analyzed. Two different operating modes are recommended, and an optimal zero-sequence voltage is designed to increase the dc voltage utilization capability of the inverter. At last, the feasibility of the proposed operation and control schemes are verified by experiments.

[5] **S. Sharma, M. Aware, and A. Bhowate**, proposes an on-board charger for the electric vehicles (EVs) by integrating the drive-train components into the charging process. The stator windings of three-phase induction motor (IM) can be used as a grid interfacing inductor with the constraint that the rotor should be in the stationary position during the charging mode. This article proposes the stator winding configurations of three-phase IM split into two equal parts at zero electrical degree for the on-board integrated battery charger. The effective filtering with these two three-phase windings combination, either in series or parallel while the rotor is in a stationary position, is analyzed. The equivalent inductance provided by stator windings for filtering is increased by generating the pulsating magnetic field (PMF) in the motor. However, it results in the unbalanced impedances in filter causing odd harmonics in the grid current. This is resolved by using a modified double synchronous reference frame control algorithm, which maintains the balanced current operation with the unity power factor at the grid interface during the charging mode. This configuration is obtained by using the existing three-phase-based drive-train components, thereby providing the saving in space and reducing the weight of EV.

[6] **M. Tong, M. Cheng, and W. Hua**, proposes to solve the existing problems in general on-board integrated chargers (IC), a novel single-phase on-board two-stage integrated charger is proposed by

taking the unique advantages of the five-phase hybrid-excitation flux-switching (HEFS) motors. The general topologies and newly presented ICs are reviewed firstly, and three main problems are concluded. Then, the proposed two-stage IC is presented, and all winding selections are thoroughly investigated by theoretical analysis, finite-element analysis (FEA) and experiments. In the proposed topology, the existing problems are all solved by employing this multi-phase system, making the reasonable winding selection, and reconfiguring the field winding. After that, a control method for charge mode and two current balance control methods are developed. The simulation results verify the effectiveness of the proposed control methods. Finally, based on a 5-kW five-phase HEFS prototype machine and two sets of the 3-phase generic motor controller, an experiment platform is built. The experiment results agree well with the simulation results. Therefore, the feasibility of a two-stage integrated on-board charger that can operate at any voltage level is confirmed, where only the hybrid-exciting machine and its own driving system are used without any additional power devices.

[7] **S.Wang and P.W. Lehn**, proposes a three-phase EV charger integrated with the dual-inverter drive. Integrated charging can substantially reduce the charging station costs by reusing drivetrain components, such as power electronics and cooling systems, for charging when the EV is parked. The dual-inverter drive allows for significant current ripple reduction throughout the charger. Operation and control of the presented charger are discussed while functionality is experimentally verified with a 10- kW -rated prototype. The prototype is able to perform constant current, constant voltage (CCCV) charging of two isolated energy storage units (ESUs) from a three-phase grid with >0.99 power factor. Charging is performed with balanced dc current passing through the dual-inverter's motor windings to prevent torque generation during charging. The prototype achieves a peak efficiency of >94% while meeting grid current harmonic standards set by International Electrotechnical Commission (IEC)-61000-3-12.

1.3 EXISTING METHOD:

In existing system, EDROC topology with three-phase drive, EDROC with the capability of active filter and d-a split-windings machine was employed to construct an EDROC. An EDROC with the capability of active filter is to address pulsating power at twice of the line frequency. And a split-windings machine is employed to construct an EDROC in to bypass the issue of generating non-negligible torque.

1.3.1 DISADVANTAGES:

- Less fault tolerant capacity
- Less grid voltage quality
- Bulky Components

1.4 PROPOSED SYSTEM:

In this System a novel electric-drive-reconstructed onboard charger (EDROC) is proposed for the solar-powered electric vehicle that incorporates a six-phase machine drive. The power traction inverter and the machine are re-leveraged to implement charging operation, further minimizing the incremental mass accordingly. In particular, charging and driving operations can be simultaneously carried out via the vehicle-roof photovoltaic panels, significantly expanding EV mileage range.

1.4.1 SYSTEM CONFIGURATION

Application Software: MATLAB/Simulink Software (R2018a)

1.4.2 ADVANTAGES

- High fault tolerating capacity
- Voltage quality is improved
- Smaller and cheaper
- Highly reliable
- Smooth torque production
- Simultaneous charging while driving

1.5 APPLICATIONS:

Electric Vehicle Charging Station

1.6 OBJECTIVE OF THE PROJECT:

The main objective of this project is to examine the impacts of voltage disturbance on EV batteries and charging systems, and provides a fault ride-through capability (FRTC) to enhance the voltage quality

1.7 ORGANIZATION OF THE PROJECT:

The project has been organized into SIX chapters. Following the chapter on introduction, architecture, objectives and applications of the project, the rest of the project outlined as follows.

Chapter 2 explains about the solar PV and battery

Chapter 3 explains about DC – AC converter and PMSM motor

Chapter 4 explains about electric vehicles

Chapter 5 explains about the topology of proposed EDROC system

Chapter 6 explains all the simulation results which are found using MATLAB/ SIMULINK

CHAPTER 2

SOLAR PV AND BATTERY

2.1 INTRODUCTION:

Photovoltaics (PV) converts light into electricity using semiconducting materials that exhibit the photovoltaic effect, a phenomenon studied in physics, photochemistry, and electrochemistry. A typical photovoltaic system employs solar panels, each comprising a number of solar cells, which generate electrical power. PV installations may be ground-mounted, rooftop mounted or wall mounted. The mount may be fixed, or use a solar tracker to follow the sun across the sky.

The operation of solar PV generates no pollution. The direct conversion of sunlight to electricity occurs without any moving parts. Photovoltaic systems have been used for fifty years in specialized applications, standalone and grid-connected PV systems have been in use for more than twenty years. They were first mass-produced in 2000, when German environmentalists and the Eurosolar organization got government funding for a ten thousand roof program. PV systems have the major disadvantage that the power output is dependent on direct sunlight, so about 10-25% is lost if a tracking system is not used, since the cell will not be directly facing the sun at all times. Dust, clouds, and other things in the atmosphere also diminish the power output. This may be made up by other power sources, usually hydrocarbon.

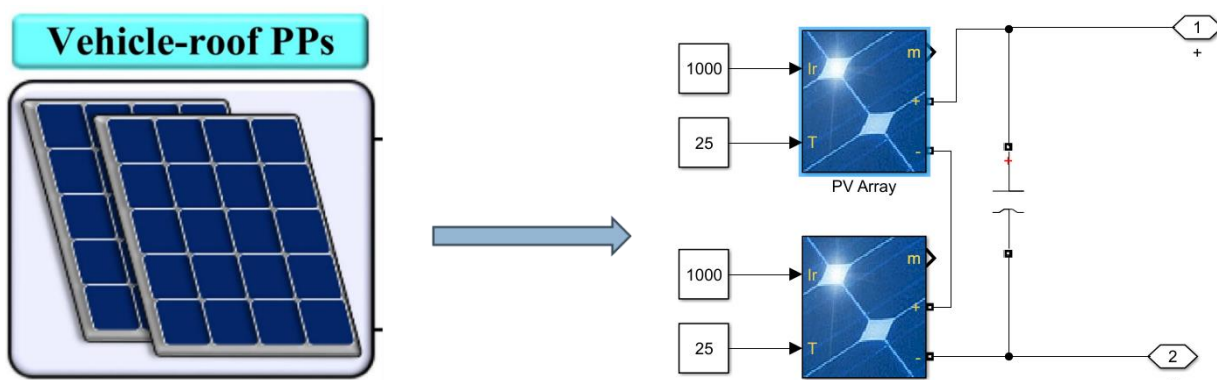


Fig. 2.1. Solar PV array

Advances in technology and increased manufacturing scale have reduced the cost, increased the reliability, and increased the efficiency of photovoltaic installations. Net metering and financial incentives, such as preferential feed-in tariffs for solar-generated electricity, have supported solar PV installations in many countries. More than 100 countries now use solar PV.

After hydro and wind powers, PV is the third renewable energy source in terms of globally capacity. In

2014, worldwide installed PV capacity increased to 177 gigawatts (GW), which is two percent of global electricity demand. China, followed by Japan and the United States, is the fastest growing market, while Germany remains the world's largest producer, with solar PV providing seven percent of annual domestic electricity consumption. With current technology (as of 2013), photovoltaics recoups the energy needed to manufacture them in 1.5 years in Southern Europe and 2.5 years in Northern Europe.

Solar cells:

Photovoltaics are best known as a method for generating electric power by using solar cells to convert energy from the sun into a flow of electrons. The photovoltaic effect refers to photons of light exciting electrons into a higher state of energy, allowing them to act as charge carriers for an electric current. The photovoltaic effect was first observed by Alexandre-Edmond Becquerel in 1839. The term photovoltaic denotes the unbiased operating mode of a photodiode in which current through the device is entirely due to the transduced light energy. Virtually all photovoltaic devices are some type of photodiode. Solar cells produce direct current electricity from sunlight which can be used to power equipment or to recharge a battery. The first practical application of photovoltaics was to power orbiting satellites and other spacecraft, but today the majority of photovoltaic modules are used for grid connected power generation. In this case an inverter is required to convert the DC to AC. There is a smaller market for off-grid power for remote dwellings, boats, recreational vehicles, electric cars, roadside emergency telephones, remote sensing, and cathodic protection of pipelines.

Photovoltaic power generation employs solar panels composed of a number of solar cells containing a photovoltaic material. Materials presently used for photovoltaics include monocrystalline silicon, polycrystalline silicon, amorphous silicon, cadmium telluride, and copper indium gallium selenide/sulfide. Copper solar cables connect modules (module cable), arrays (array cable), and sub-fields. Because of the growing demand for renewable energy sources, the manufacturing of solar cells and photovoltaic arrays has advanced considerably in recent years.

Solar photovoltaics power generation has long been seen as a clean energy technology which draws upon the planet's most plentiful and widely distributed renewable energy source – the sun. The technology is "inherently elegant" in that the direct conversion of sunlight to electricity occurs without any moving parts or environmental emissions during operation. It is well proven, as photovoltaic systems have now been used for fifty years in specialized applications, and grid-connected systems have been in use for over twenty years.

Cells require protection from the environment and are usually packaged tightly behind a glass

sheet. When more power is required than a single cell can deliver, cells are electrically connected together to form photovoltaic modules, or solar panels. A single module is enough to power an emergency telephone, but for a house or a power plant the modules must be arranged in multiples as arrays.

Photovoltaic power capacity is measured as maximum power output under standardized test conditions (STC) in "W_p" (watts peak). The actual power output at a particular point in time may be less than or greater than this standardized, or "rated," value, depending on geographical location, time of day, weather conditions, and other factors. Solar photovoltaic array capacity factors are typically under 25%, which is lower than many other industrial sources of electricity.

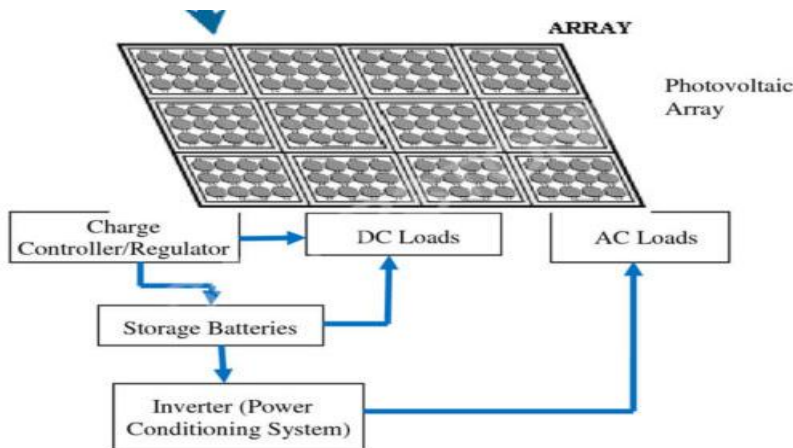


Fig. 2.2. Array flow diagram

Electrical efficiency (also called conversion efficiency) is a contributing factor in the selection of a photovoltaic system. However, the most efficient solar panels are typically the most expensive, and may not be commercially available. Therefore, selection is also driven by cost efficiency and other factors.

2.2 EFFICIENCY:

The electrical efficiency of a PV cell is a physical property which represents how much electrical power a cell can produce for a given insolation. The basic expression for maximum efficiency of a photovoltaic cell is given by the ratio of output power to the incident solar power (radiation flux times area). The efficiency is measured under ideal laboratory conditions and represents the maximum achievable efficiency of the PV material. Actual efficiency is influenced by the output Voltage, current, junction temperature, light intensity and spectrum. The most efficient type of solar cell to date is a multi-junction concentrator solar cell with an efficiency of 46.0% produced by Fraunhofer ISE in December 2014. The highest efficiencies achieved without concentration include a material by Sharp

Corporation at 35.8% using a proprietary triple-junction manufacturing technology in 2009, and Boeing Spectrolab (40.7% also using a triple-layer design). The US company SunPower produces cells that have an efficiency of 21.5%, well above the market average of 12–18%. There is an ongoing effort to increase the conversion efficiency of PV cells and modules, primarily for competitive advantage. In order to increase the efficiency of solar cells, it is important to choose a semiconductor material with an appropriate band gap that matches the solar spectrum. This will enhance the electrical and optical properties. Improving the method of charge collection is also useful for increasing the efficiency. There are several groups of materials that are being developed. Ultrahigh-efficiency devices ($\eta > 30\%$) are made by using GaAs and GaInP₂ semiconductors with multijunction tandem cells. High-quality, single-crystal silicon materials are used to achieve high-efficiency, low cost cells ($\eta > 20\%$).

Recent developments in Organic photovoltaic cells (OPVs) have made significant advancements in power conversion efficiency from 3% to over 15% since their introduction in the 1980s.^[30] To date, the highest reported power conversion efficiency ranges from 6.7% to 8.94% for small molecule, 8.4%–10.6% for polymer OPVs, and 7% to 21% for perovskite OPVs. OPVs are expected to play a major role in the PV market. Recent improvements have increased the efficiency and lowered cost, while remaining environmentally-benign and renewable.

Several companies have begun embedding power optimizers into PV modules called smart modules. These modules perform maximum power point tracking (MPPT) for each module individually, measure performance data for monitoring, and provide additional safety features. Such modules can also compensate for shading effects, wherein a shadow falling across a section of a module causes the electrical output of one or more strings of cells in the module to decrease.

One of the major causes for the decreased performance of cells is overheating. The efficiency of a solar cell declines by about 0.5% for every 1 degree Celsius increase in temperature. This means that a 100 degree increase in surface temperature could decrease the efficiency of a solar cell by about half. Self-cooling solar cells are one solution to this problem. Rather than using energy to cool the surface, pyramid and cone shapes can be formed from silica, and attached to the surface of a solar panel. Doing so allows visible light to reach the solar cells, but reflects infrared rays (which carry heat).

2.2.1 APPLICATIONS:

A photovoltaic system, or solar PV system is a power system designed to supply usable solar power by means of photovoltaics. It consists of an arrangement of several components, including solar panels to absorb and directly convert sunlight into electricity, a solar inverter to change the electric current from DC to AC, as well as mounting, cabling and other electrical accessories. PV systems range from

small, roof-top mounted or building-integrated systems with capacities from a few to several tens of kilowatts, to large utility-scale power stations of hundreds of megawatts. Nowadays, most PV systems are grid-connected, while stand-alone systems only account for a small portion of the market.

2.2.2 ADVANTAGES:

- The 122 PW of sunlight reaching the Earth's surface is plentiful—almost 10,000 times more than the 13 TW equivalent of average power consumed in 2005 by humans. This abundance leads to the suggestion that it will not be long before solar energy will become the world's primary energy source. Additionally, solar electric generation has the highest power density (global mean of 170 W/m²) among renewable energies.
- Solar power is pollution-free during use. Production end-wastes and emissions are manageable using existing pollution controls. End-of-use recycling technologies are under development and policies are being produced that encourage recycling from producers.
- PV installations can operate for 100 years or even more with little maintenance or intervention after their initial set-up, so after the initial capital cost of building any solar power plant, operating costs are extremely low compared to existing power technologies.
- Grid-connected solar electricity can be used locally thus reducing transmission/distribution losses (transmission losses in the US were approximately 7.2% in 1995).

Compared to fossil and nuclear energy sources, very little research money has been invested in the development of solar cells, so there is considerable room for improvement. Nevertheless, experimental high efficiency solar cells already have efficiencies of over 40% in case of concentrating photovoltaic cells and efficiencies are rapidly rising while mass-production costs are rapidly falling.

2.3 BATTERY:

An electric battery is a source of electric power consisting of one or more electrochemical cells with external connections for powering electrical devices. When a battery is supplying electric power, its positive terminal is the cathode and its negative terminal is the anode. The terminal marked negative is the source of electrons that will flow through an external electric circuit to the positive terminal. When a battery is connected to an external electric load, a redox reaction converts high-energy reactants to lower-energy products, and the free-energy difference is delivered to the external circuit as electrical energy. Historically the term "battery" specifically referred to a device composed of multiple cells; however, the usage has evolved to include devices composed of a single cell.

Primary (single-use or "disposable") batteries are used once and discarded, as

the electrode materials are irreversibly changed during discharge; a common example is the alkaline battery used for flashlights and a multitude of portable electronic devices.

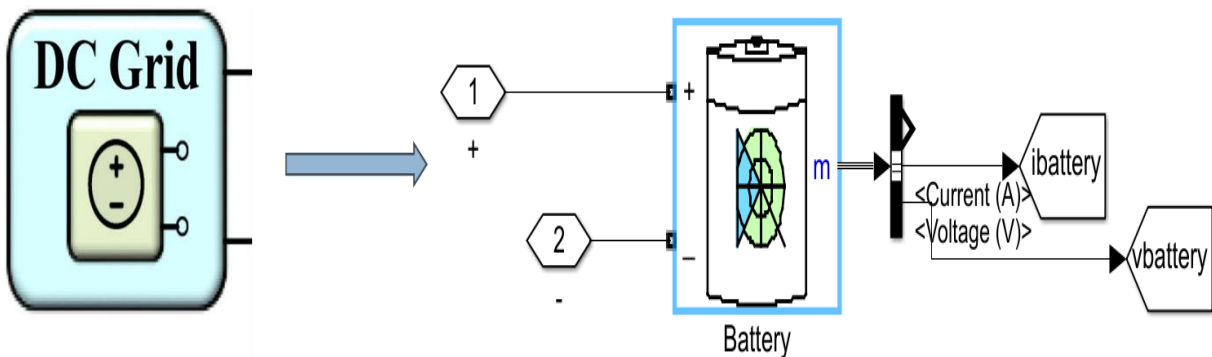


Fig. 2.3. DC Grid system

Secondary re-chargeable battery can be discharged and recharged multiple times using an applied electric current; the original composition of the electrodes can be restored by reverse current. Examples include the lead-acid batteries used in vehicles and lithium-ion batteries used for portable electronics such as laptops and mobile phones.

Batteries come in many shapes and sizes, from miniature cells used to power hearing aids and wristwatches to small, thin cells used in smartphones, to large lead acid batteries or lithium-ion batteries in vehicles, and at the largest extreme, huge battery banks the size of rooms that provide standby or emergency power for telephone exchanges and computer data centers.

Batteries have much lower specific energy (energy per unit mass) than common fuels such as gasoline. In automobiles, this is somewhat offset by the higher efficiency of electric motors in converting electrical energy to mechanical work, compared to combustion engines.

2.3.1 LITHIUM-ION BATTERY:

A lithium-ion battery or Li-ion battery is a type of rechargeable battery in which lithium ions move from the negative electrode through an electrolyte to the positive electrode during discharge and back when charging. Li-ion batteries use an intercalated lithium compound as the material at the positive electrode and typically graphite at the negative electrode.

Li-ion batteries have a high energy density, no memory effect (other than LFP cells) and low self-discharge. Cells can be manufactured to either prioritize energy or power density.^[10] They can however be a safety hazard since they contain flammable electrolytes and if damaged or incorrectly charged can lead to explosions and fires.

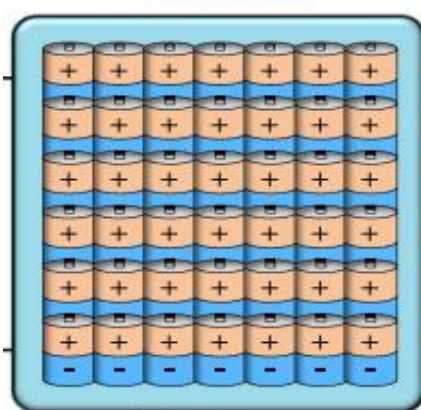


Fig. 2.4. Battery(Rechargeable)

A prototype Li-ion battery was developed by Akira Yoshino in 1985, based on earlier research by John Goodenough, M. Stanley Whittingham, Rachid Yazami and Koichi Mizushima during the 1970s–1980s, and then a commercial Li-ion battery was developed by a Sony and Asahi Kasei team led by Yoshio Nishi in 1991. Lithium-ion batteries are commonly used for portable electronics and electric vehicles and are growing in popularity for military and aerospace applications.

Chemistry, performance, cost and safety characteristics vary across types of lithium-ion batteries. Handheld electronics mostly use lithium polymer batteries (with a polymer gel as electrolyte), a lithiumcobaltoxide(LiCoO_2) cathode material, and a graphite anode, which together offer a high energy density. Lithiumironphosphate(LiFePO_4), lithiummanganeseoxide(LiMn_2O_4 spinel, or Li_2MO_3 -based lithium rich layered materials, LMR-NMC), and lithium nickel manganese cobalt oxide(LiNiMnCoO_2 or NMC) may offer longer lives and may have better rate capability. Such batteries are widely used for electric tools, medical equipment, and other roles. NMC and its derivatives are widely used in electric vehicles.

Research areas for lithium-ion batteries include extending lifetime, increasing energy density, improving safety, reducing cost, and increasing charging speed,^[18] among others. Research has been under way in the area of non-flammable electrolytes as a pathway to increased safety based on the flammability and volatility of the organic solvents used in the typical electrolyte. Strategies include aqueous lithium-ion batteries, ceramic solid electrolytes, polymer electrolytes, ionic liquids, and heavily fluorinated systems.

2.3.2 HISTORY:

Research on rechargeable Li-ion batteries dates to the 1960s; one of the earliest examples is a CuF₂/Li battery developed by NASA in 1965. The breakthrough that produced the earliest form of the modern Li-ion battery was made by British chemist M. Stanley Whittingham in 1974, who first used titanium disulfide (TiS₂) as a cathode material, which has a layered structure that can take in lithium ions without significant changes to its crystal structure. Exxon tried to commercialize this battery in the late 1970s, but found the synthesis expensive and complex, as TiS₂ is sensitive to moisture and releases toxic H₂S gas on contact with water. More prohibitively, the batteries were also prone to spontaneously catching fire due to the presence of metallic lithium in the cells. In 1980, Koichi Mizushima and John B. Goodenough, after testing a range of alternative materials, replaced TiS₂ with lithium cobalt oxide (LiCoO₂, or LCO), which has a similar layered structure but offers a higher voltage and is much more stable in air. This material would later be used in the first commercial Li-ion battery, although it did not, on its own, resolve the persistent issue of flammability.^[23] The same year, Rachid Yazami demonstrated the reversible electrochemical intercalation of lithium in graphite,^{[24][25]} and invented the lithium graphite electrode (anode).

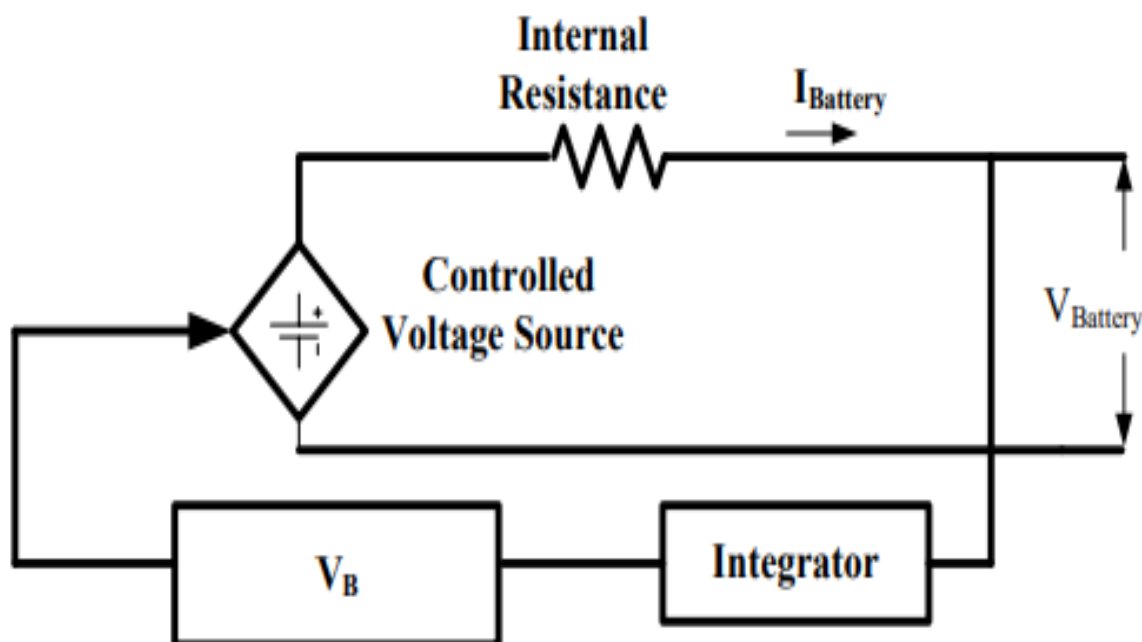


Fig.2.5. Battery mode

These early attempts to develop rechargeable Li-ion batteries used lithium metal anodes, which were ultimately abandoned due to safety concerns, as lithium metal is unstable and prone to dendrite formation, which can cause short-circuiting. The eventual solution was to use an intercalation anode, similar to that used for the cathode, which prevents the formation of lithium metal during battery charging. A variety of anode materials were studied; in 1987, Akira Yoshino patented what would become the first commercial lithium-ion battery using an anode of "soft carbon" (a charcoal-like material) along with Goodenough's previously reported LCO cathode and a carbonate ester-based electrolyte. In 1991, using Yoshino's design, Sony began producing and selling the world's first rechargeable lithium-ion batteries. The following year, a joint venture between Toshiba and Asashi Kasei Co. also released their own lithium-ion battery.

Significant improvements in energy density were achieved in the 1990s by replacing the soft carbon anode first with hard carbon and later with graphite, a concept originally proposed by Jürgen Otto Besenhard in 1974 but considered unfeasible due to unresolved incompatibilities with the electrolytes then in use. In 2012 John B. Goodenough, Rachid Yazami and Akira Yoshino received the 2012 IEEE Medal for Environmental and Safety Technologies for developing the lithium ion battery; Goodenough, Whittingham and Yoshino were awarded the 2019 Nobel Prize in Chemistry "for the development of lithium ion batteries". In 2010, global lithium-ion battery production capacity was 20 gigawatt-hours. By 2016, it was 28 GWh, with 16.4 GWh in China. Production in 2021 is estimated by various sources to be between 200 and 600 GWh, and predictions for 2023 range from 400 to 1,100 GWh.

CHAPTER 3

DC-AC CONVERTER AND PMSM

3.1 DC-AC CONVERTER:

3.1.1 INTRODUCTION TO POWER ELECTRONICS:

Power electronic inverters, especially DC-AC Pulse width modulated inverters have been extending their range of use in industrial application which are reduced energy consumption, better system efficiency, improved quality of product, good maintenance, and so on. For a medium voltage grid, it is troublesome to connect only one power semiconductor switches directly. As a result, a multilevel inverter structure has been introduced as an alternative solution to represent high power and medium voltage situations such as mills, conveyors, pumps, fans, blowers, compressors, and other appliances. As a cost-effective solution, multilevel inverter not only achieves high power ratings, but also enables the use of low power application in renewable energy sources such as photovoltaic, wind, and fuel cells which can be easily integrated to a multilevel inverter system for a high-power application. The inverters in such application areas as stated above should be able to handle high voltage and maximum power. For this reason, two level high voltage and maximum power inverters have been designed with series connection of switching power devices such as Gate-Turn-Off Thyristors (GTOs), Integrated Gate Commutated Transistors (IGCTs), and Insulated Gate Bipolar Transistors (IGBTs), because the series connection allows reaching much higher voltages.

The circuit works on the series connection of switching power devices creates serious problems occur during unequal power distribution in the load. As alternatives to effectively solve the above-mentioned problems, different circuit topologies of multilevel inverter and converter have been modelled and employed. The output voltage of the multilevel inverter has many levels produced from DC voltage source. The quality of the output voltage is improved as the number of voltage levels increase and reduced the filter size. The cascaded multilevel inverter has employed due to the maximum demand of medium voltage high power inverters. This multilevel inverter topology can extend rated inverter voltage and power by increasing the stepped voltage levels. They can also increase equivalent switching frequency without increase of actual switching frequency, thus reducing ripple component of inverter output voltage and Electromagnetic Interference (EMI effects). In this concept, to extend the power supply, the review of the total harmonic distortion has to be reduced and improved, for the performance of the system. This chapter described the multilevel inverter concept and detailed study of current source inverter.

3.1.2 VOLTAGE SOURCE INVERTER:

Fig 3.2.1 shows the three-phase voltage-source inverter structure. A DC voltage source supported by a relatively large capacitor feeds the 3-phase inverter circuit. The DC voltage source can be a battery, fuel-cell stack, diode rectifier, and/or capacitor. Six switches are used in the main circuit; each is traditionally composed of a power transistor and an antiparallel (or freewheeling) diode to provide bidirectional current flow and unidirectional voltage blocking capability. It has certain limitation of the voltage source inverter. The AC output voltage is limited below and cannot exceed the DC voltage. The V-source inverter is a buck (step-down) inverter for DC-to-AC power conversion. The upper and lower devices of each phase leg should not be gated on simultaneously because a shoot-through would occur and destroy the devices. The shoot-through problem by electromagnetic interference (EMI) noise's misgating-on is a major killer to the converter's reliability.

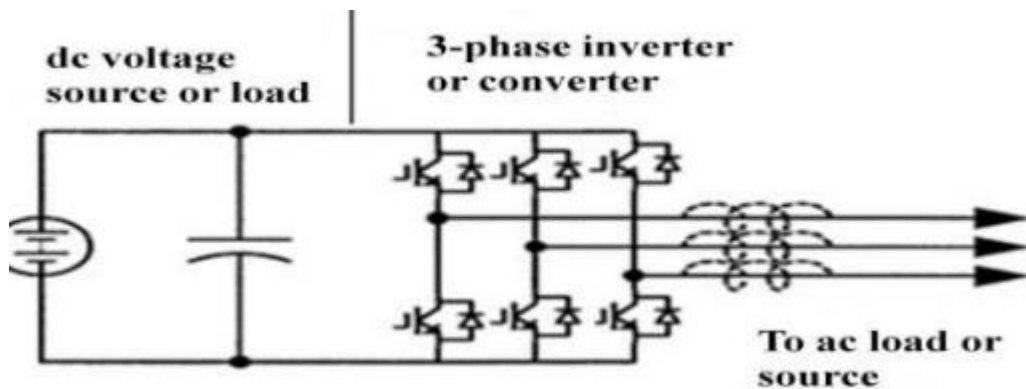


Fig. 3.1 Voltage-Source Inverter

3.1.3 CURRENT SOURCE INVERTER:

The three-phase current-source inverter structure. A DC current source feeds the 3 phase inverter circuit. The DC current source can be a relatively large DC inductor fed by a voltage source such as a battery, fuel-cell stack, diode rectifier, or thyristor converter. Six switches are used in the main circuit each is traditionally composed of a semiconductor switching device with reverse block capability such as a Gate-Turn-Off Thyristor (GTO) and SCR or a power transistor with a series diode to provide unidirectional current flow and bidirectional voltage blocking. The main switches of the I-source inverter have to block reverse voltage that requires a series diode to be used in combination with high-speed and high performance transistors such as insulated gate bipolar transistors (IGBTs). This prevents the direct use of low-cost and high performance IGBT modules.

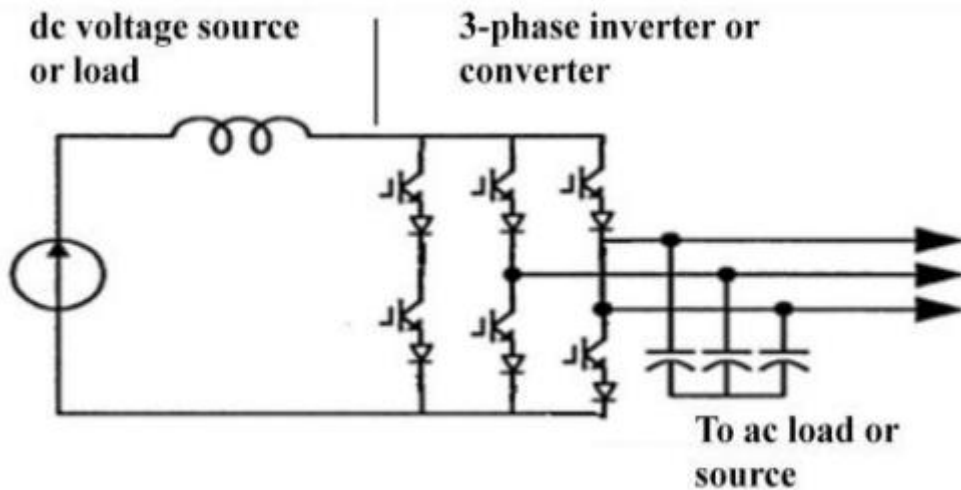


Fig. 3.2. Current-source inverter

The current source inverter has certain limitations of the AC output voltage that has to be greater than the original DC voltage that feeds the DC inductor or the DC voltage produced is always smaller than the AC input voltage. The CSI is a boost inverter for DC-to-AC power conversion. At least one of the upper devices and one of the lower devices have to be gated on and maintained on at any time. Otherwise, an open circuit of the DC inductor would occur and destroy the devices. The open-circuit problem by EMI noise's misgating-off is a major concern of the inverters reliability. The main switches of the I-source inverter have to block reverse voltage that requires a series diode to be used in combination with high-speed and high performance transistors such as insulated gate bipolar transistors (IGBTs). This prevents the direct use of low-cost and high performance IGBT modules and intelligent power modules (IPMs). The circuit works on the series connection of switching power devices creates serious problems occur during unequal power distribution in the load. As alternatives to effectively solve the above-mentioned problems, different circuit topologies of multilevel inverter and converter have been modelled and employed. The output voltage of the multilevel inverter has many levels produced from DC voltage source. The quality of the output voltage is improved as the number of voltage levels increase and reduced the filter size. The cascaded multilevel inverter has employed due to the maximum demand of medium voltage high power inverters. This multilevel inverter topology can extend rated inverter voltage and power by increasing the stepped voltage levels.

3.2 PERMANENT MAGNET SYNCHRONOUS MOTOR:

3.2.1 INTODUCTION TO PMSM CONSTRUCTION AND WORKING:

The relevant rotor configuration of PM synchronous machines and their impact on the direct and quadrature axis inductance and the distinct difference between the PM brushless dc and synchronous machines are discussed.

3.2.2 MACHINE CONFIGURATIONS/CONSTRUCTION:

The permanent magnet (PM) synchronous machines can be broadly classified. The PMSMs are classified as follows:

On the basis of the direction of field flux

- i. Radial field: the flux direction is along the radius of the machine.
- ii. Axial field: the flux direction is parallel to the rotor shaft.

Depending on the wave shape of induced emf

- i. Brushless dc machines with trapezoidal emf waveforms.
- ii. PMSM with sinusoidal waveform.

The radial –field PM machines are common: the axial-field machines are coming into prominence in a small number of applications because of their higher power density and acceleration. Note that these are very desirable features in highperformance applications. The magnets can be placed in many ways on the rotor. The high-power-density synchronous machines have surface PMs with redial orientation intended generally for low speed applications, whereas the interior-magnet version is for high-speed applications. Regardless of the manner of mounting the PMs, the basic principle of operation is the same. An important consequence of the method of mounting the rotor magnets is the difference in direct and quadrature axes inductance values. It is explained as follows. The rotor magnetic axis is called direct axis and the principle path of the flux is through the magnets. The permeability of high-flux-density permanent magnets is almost that of the air. This result in the magnet thickness becoming an extension of air gap by that amount. The stator inductance when the direct axis or magnets are aligned with the stator winding is known as direct axis inductance. By rotating the magnets from the aligned position by 90 degrees, the stator flux sees the interpolar area of the rotor containing only the iron path, and the inductance measured in the position is referred to as quadrature axis inductance [29]. Generally the direct axis reluctance is greater than the quadrature-axis reluctance because the effective air gap of the direct axis is in multiples of that of the actual air gaps seen by the quadrature axis. The consequence of such an unequal reluctance is that $L_d < L_q$.

Where L_d is the inductance along the magnet axis (i.e., direct axis) and L_q is the inductance along an axis in quadrature to the magnet axis. This is quite contrary to the wound-rotor salient-pole synchronous machines. Where the quadrature-axis inductance is always greater than the direct-axis inductance. Note that, in the wound-rotor salient-pole synchronous machine, the direct axis, having the excitation coils, has a small air gap, whereas the quadrature axis has the large air gap. Fig. 3.1(i) shows the magnets mounted on the surface of the outer periphery of rotor laminations. This arrangement provides the highest air gap flux density, but it has the drawback of lower structural integrity and mechanical robustness. Machines with this arrangement of magnets are known as surface mount PMSMs. They are not preferred for high-speed applications, generally greater than 3,000 rpm. There is very little (less than 10%) variation between the quadrature and direct-axis inductances in this machine. This particular fact has consequences for the control, operation and characteristics of the surface-mount PMSM drives.

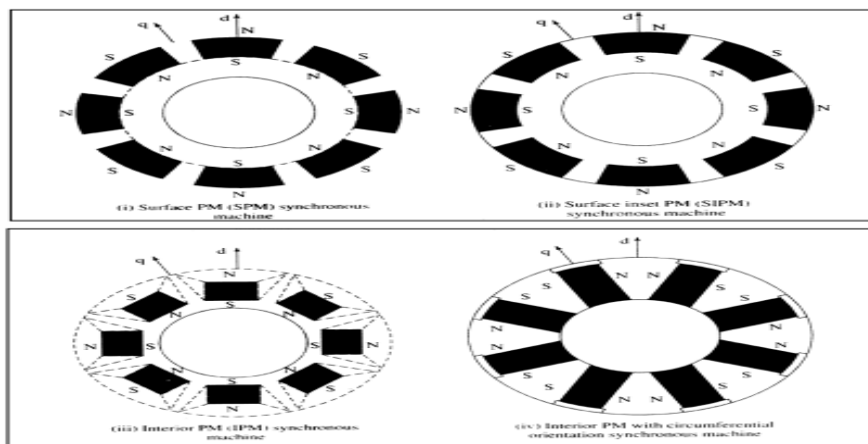


Fig. 3.3. Surface-PM (SPM) Synchronous Machine

the magnet placed in the grooves of the outer periphery of the rotor lamination, providing a uniform cylindrical surface of rotor. Such a type of arrangement is more robust mechanically compared to surface-mount machines. The ratio between the quadrature- and direct-axis inductance can be as high as 2 to 2.5 in this machine. This construction is known as inset PM synchronous machine. Fig. 3.2 (iii) and (iv) shows the placement of magnets in the middle of the rotor laminations in radial and circumferential orientations, respectively. This construction is mechanically robust and therefore suited for high speed application. The manufacturing of this arrangement is more complex than for surface mount or inset-magnet rotor. Note that the ratio between the quadrature- and direct-axis inductance can be higher than that of the inset-magnet rotor but generally does not exceed three in value. This type of machine construction is generally referred to as interior PMSM.

3.2.3 FLUX-DENSITY DISTRIBUTION:

The flux plot and flux density vs. rotor position of a surface PM with radial orientation are shown in Fig. 3.2 and 3.3, respectively. The dips in the flux density at various point occurs because of the slot opening of the lamination where the reluctance is much higher and, hence. The flux and its density are lower. The slotting effect also affects the induced emfs in the machine armature, clearly raising design and practical concerns about possible ripple effects. The slotting effect exists regard-less of whether the machine is designed with sinusoidal or trapezoidal fluxdensity distribution. For these distributions, predetermined sinusoidal or rectangular cur-rents are injected to produce the torque. Invariably, that result in ripple air gap torque capable of causing undesirable effect at low speed.

3.2.4 LINE-START PM SYNCHRONOUS MACHINES:

Some PM synchronous machines are intended and designed for constant-speed applications, to improve efficiency and power factor in comparison to induction and wound-rotor synchronous motors. Variable-speed PM synchronous motors drives have no need for the damper windings to offset hunting and oscillation. The damping is provide by properly controlling the input current from the inverter. This result in a compact and a smaller rotor than of the machine with damper windings. The way damping is produced in the PM synchronous motor with and without damper windings deserves a comment. The machine with the damper windings operates to suppress the oscillations with no external feedback. The feedback comes internally through the induced emf due to the slip speed in the cage windings. In the inverter-controlled PM drive, the control has to be initiated by an external signal or feedback variable to counter the oscillation. It dependence on an external feedback loop compromises reliability. Wherever reliable operation regardless of the accuracy in speed control is a major concern or requirement, the synchronous motor with damper windings might prove to be an intelligent choice.

3.2.5 VARIOUS CONTROL STRATEGIES OF PMSM:

The most common five different control strategies used for PMSM control are :

- (1) Constant torque angle control.
- (2) Optimum torque per ampere control.
- (3) Unity power factor control.
- (4) Constant mutual air gap flux linkages control.
- (5) Angle control of air gap flux and current phasors. Here, the study is concentrated to Constant torque angle control and then explain the vector control or the Field Oriented Control (FOC) Method.

3.2.6 MODEL OF THE PMSM:

A dynamic model of the PMSM is required to derive the vector-control algorithm to decouple the air-flux and torque channels in the drive system. The two-axes PMSM stator winding can be considered to have equal turns per phase.

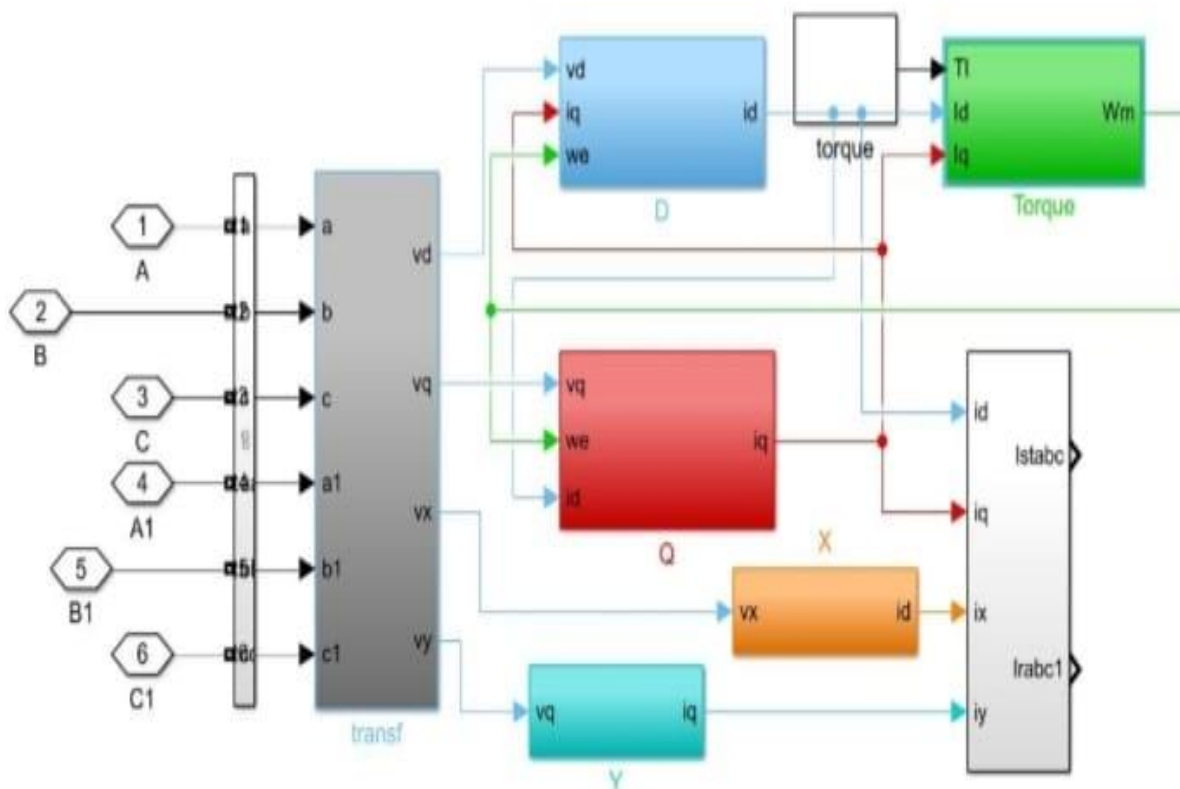


Fig.3.4. Model of the PMSM

The design of a six-phase Permanent Magnet Synchronous Motor (PMSM) in Simulink involves developing an accurate mathematical model that represents the motor's electromechanical behavior and control strategies. Unlike conventional three-phase PMSMs, six-phase motors offer advantages such as reduced torque ripple, improved fault tolerance, and enhanced power density, making them suitable for high-performance applications like electric vehicles and aerospace systems. The motor is modeled using differential equations governing voltage, flux linkage, and torque production, incorporating parameters like stator resistance, inductance, permanent magnet flux, and rotor dynamics. The six-phase configuration requires appropriate transformations, such as the extended Clarke and Park transforms, to simplify control implementation. The motor is typically driven by a six-phase voltage source inverter, which generates appropriate switching signals and torque regulation by managing the dq-axis currents in both three-phase subsystems. Simulink provides a platform to integrate these components using Simscape Electrical, allowing for simulation, analysis,

and optimization of the motor's performance under varying load and speed conditions.

The rotor flux can be concentrated along the d axis while there is zero flux along the q axis. The rotor frame of reference is chosen because the position of the rotor magnets determines independently of the stator voltages and currents, the instantaneous induced emfs and subsequently the stator currents and torque of the machine. Again this is not the case in the induction machine where the rotor fluxes are not independent variables, they are influenced by the stator voltages and currents, and that is why any frame of reference is suitable for the dynamic modeling of the induction machine. When rotor reference frames are considered, it means the equivalent q and d axis stator windings are transformed to the reference frames that are revolving at rotor speed . The consequence is that there is zero speed differential between the rotor and stator magnetic fields and the stator q and d axis windings have a fixed phase relationship with the rotor magnet axis, which is the d axis in the modeling. The stator flux-linkage equations are:

$$V_{qs} = R_q i_{qs} + p\lambda_{qs} + \omega_r \lambda_{ds}$$

$$V_{ds} = R_d i_{ds} + p\lambda_{ds} - \omega_r \lambda_{qs}$$

where Rq and Rd are the quadrature and direct axis winding resistances, which are equal (referred to as Rs) and the q and d axes stator flux linkages in the rotor reference frames are :

$$\lambda_{qs} = L_s i_{qs} + L_m i_{qr}$$

$$\lambda_{ds} = L_s i_{ds} + L_m i_{dr}$$

But the self-inductances of the stator q and d axes winding are equal to Ls only when the rotor magnets have of electrical 180°. This implies that the reluctances along the magnet axis and the interpolar axis are different when a winding (say d axis) is in alignment with the rotor magnet axis. The reluctance of the path is maximum; the magnet reluctance is almost the same as the air gap reluctance, and hence its inductance is the lowest at this time. The inductance then is referred to as the direct – axis inductance, Ld. At this instant, the q axis winding faces the inter pole path in the rotor, where the flux path encounters no magnet but only the air gaps and iron in the rotor. As the rotor magnet and the stator q and d axis winding are fixed in space that the winding inductance do not change in rotor reference frame. Hence, to compute the stator flux linkages in the q and d axis, the 47 permanent magnetic excitation is modeled as a constant current source say ifr

CHAPTER-4

ELECTRIC VEHICLES

4.1 INTRODUCTION:

Electric vehicle (EV) is a vehicle that uses one or more electric motors for propulsion. It can be powered by a collector system, with electricity from extravehicular sources, or it can be powered autonomously by a battery (sometimes charged by solar panels, or by converting fuel to electricity using fuel cells or a generator). EVs include, but are not limited to, road and rail vehicles, surface and underwater vessels, electric aircraft and electric spacecraft.

EVs first came into existence in the mid-19th century, when electricity was among the preferred methods for motor vehicle propulsion, providing a level of comfort and ease of operation that could not be achieved by the gasoline cars of the time. Internal combustion engines were the dominant propulsion method for cars and trucks for about 100 years, but electric power remained commonplace in other vehicle types, such as trains and smaller vehicles of all types.

In the 21st century, EVs have seen a resurgence due to technological developments, and an increased focus on renewable energy and the potential reduction of transportation's impact on climate change, air pollution, and other environmental issues. Project Drawdown describes electric vehicles as one of the 100 best contemporary solutions for addressing climate change.

Government incentives to increase adoption were first introduced in the late 2000s, including in the United States and the European Union, leading to a growing market for the vehicles in the 2010s. Increasing public interest and awareness and structural incentives, such as those being built into the green recovery from the COVID-19 pandemic, is expected to greatly increase the electric vehicle market. The International Energy Agency said in 2021 that governments should do more to meet climate goals, including policies for heavy electric vehicles. Electric vehicle sales may increase from 2% of global share in 2016 to 30% by 2030. Much of this growth is expected in markets like North America, Europe and China; a 2020 literature review suggested that growth in use of electric 4-wheeled vehicles appears economically unlikely in developing economies, but that electric 2-wheeler growth is likely. There are more 2 and 3 wheel EVs than any other type. leading to a growing market for the vehicles in the 2010s. Increasing public interest and awareness and structural incentives, such as those being built into the green recovery

4.2 HISTORY:

Electric motive power started in 1827, when Hungarian priest Ányos Jedlik built the first crude but viable electric motor, provided with stator, rotor and commutators; the next year, he used it to power a tiny car. In 1835, professor Sibrandus Stratingh of the University of Groningen, the Netherlands, built a small-scale electric car, and between 1832 and 1839 (the exact year is uncertain), Robert Anderson of Scotland invented the first crude electric carriage, powered by non-rechargeable primary cells. American blacksmith and inventor Thomas Davenport built a toy electric locomotive, powered by a primitive electric motor, in 1835. In 1838, a Scotsman named Robert Davidson built an electric locomotive that attained a speed of four miles per hour (6 km/h). In England a patent was granted in 1840 for the use of rails as conductors of electric current, and similar American patents were issued to Lilley and Colten in 1847.

The first mass-produced electric vehicles appeared in America in the early 1900s. In 1902, the Studebaker Automobile Company entered the automotive business with electric vehicles, though it also entered the gasoline vehicles market in 1904. However, with the advent of cheap assembly line cars by Ford Motor Company, the popularity of electric cars declined significantly. Due to the limitations of storage batteries at that time, electric cars did not gain much popularity; however, electric trains gained immense popularity due to their economies and achievable speeds. By the 20th century, electric rail transport became commonplace due to advances in the development of electric locomotives. Over time their general-purpose commercial use reduced to specialist roles as platform trucks, forklift trucks, ambulances, tow tractors and urban delivery vehicles, such as the iconic British milk float; for most of the 20th century, the UK was the world's largest user of electric road vehicles. Electrified trains were used for coal transport, as the motors did not use precious oxygen in the mines. Switzerland's lack of natural fossil resources forced the rapid electrification of their rail network. One of the earliest rechargeable batteries – the nickel-iron battery – was favoured by Edison for use in electric cars.

EVs were among the earliest automobiles, and before the pre-eminence of light, powerful internal combustion engines, electric automobiles held many vehicle land speed and distance records in the early 1900s. They were produced by Baker Electric, Columbia Electric, Detroit Electric, and others, and at one point in history out-sold gasoline-powered vehicles. In 1900, 28 percent of the cars on the road in the US were electric. EVs were so popular that even

President Woodrow Wilson and his secret service agents toured Washington, D.C. in their Milburn Electrics, which covered 60–70 mi (100–110 km) per charge.

A number of developments contributed to a decline in the popularity of electric cars.^[18] Improved road infrastructure required a greater range than that offered by electric cars, and the discovery of large reserves of petroleum in Texas, Oklahoma, and California led to the wide availability of affordable gasoline/petrol, making internal combustion powered cars cheaper to operate over long distances.^[19] Also, internal combustion powered cars became ever-easier to operate thanks to the invention of the electric starter by Charles Kettering in 1912, which eliminated the need of a hand crank for starting a gasoline engine, and the noise emitted by ICE cars became more bearable thanks to the use of the muffler, which Hiram Percy Maxim had invented in 1897. As roads were improved outside urban areas, electric vehicle range could not compete with the ICE. Finally, the initiation of mass production of gasoline-powered vehicles by Henry Ford in 1913 reduced significantly the cost of gasoline cars as compared to electric cars. In the 1930s, National City Lines, which was a partnership of General Motors, Firestone, and Standard Oil of California purchased many electric tram networks across the country to dismantle them and replace them with GM buses. The partnership was convicted of conspiring to monopolize the sale of equipment and supplies to their subsidiary companies, but were acquitted of conspiring to monopolize the provision of transportation services.

4.3 EXPERIMENTATION:

In January 1990, General Motors' President introduced its EV concept two-seater, the "Impact", at the Los Angeles Auto Show. That September, the California Air Resources Board mandated major-automaker sales of EVs, in phases starting in 1998. From 1996 to 1998 GM produced 1117 EV1s, 800 of which were made available through three-year leases. Chrysler, Ford, GM, Honda, and Toyota also produced limited numbers of EVs for California drivers. In 2003, upon the expiration of GM's EV1 leases, GM discontinued them. The discontinuation has variously been attributed to:

- the auto industry's successful federal court challenge to California's zero-emissions vehicle mandate,
- a federal regulation requiring GM to produce and maintain spare parts for the few thousands EV1s and
- The success of the oil and auto industries' media campaign to reduce public acceptance of EVs.

4.4 REINTRODUCTION:

During the late 20th and early 21st century, the environmental impact of the petroleum-based transportation infrastructure, along with the fear of peak oil, led to renewed interest in an electric transportation infrastructure. EVs differ from fossil fuel-powered vehicles in that the electricity they consume can be generated from a wide range of sources, including fossil fuels, nuclear power, and renewables such as solar power and wind power or any combination of those. The carbon footprint and other emissions of electric vehicles vary depending on the fuel and technology used for electricity generation. The electricity may be stored in the vehicle using a battery, flywheel, or super-capacitors. Vehicles using internal combustion engines usually derive their energy from a single or a few sources, usually non-renewable fossil fuels. A key advantage of electric vehicles is regenerative braking, which recovers kinetic energy, typically lost during friction braking as heat, and restores it to the on-board battery. The carbon footprint and other emissions of electric vehicles vary depending on the fuel and technology used for electricity generation. The electricity may be stored in the vehicle using a battery, flywheel,

4.5 ELECTRICITY SOURCES:

There are many ways to generate electricity, of varying costs, efficiency and ecological desirability. An advantage of electric vehicles is regenerative braking, which recovers kinetic energy.



Fig. 4.1. passenger train, taking power through a third rail with return through the traction rails



Fig. 4.2. An electric locomotive at Brig, Switzerland



Fig. 4.3. The MAZ-7907 uses an on-board generator to power in-wheel electric motors

4.5.1 CONNECTIONS TO GENERATOR PLANTS:

- Direct connection to generation plants as is common among electric trains, trams, trolleybuses, and trolleytrucks (See also: overhead lines, third rail and conduit current collection)
- Online electric vehicle collects power from electric power strips buried under the road surface through electromagnetic induction

4.5.2 ONBOARD GENERATORS AND HYBRID EV:

- Generated on-board using diesel engine: diesel-electric locomotive diesel-electric multiple unit
- Generated on-board using a fuel cell: fuel cell vehicle
- Generated on-board using nuclear energy: nuclear submarines and aircraft carriers
- Renewable sources such as solar power: solar vehicle

It is also possible to have hybrid EVs that derive electricity from multiple sources, such as:

- On-board rechargeable electricity storage system (RESS) and a direct continuous connection to land-based generation plants for purposes of on-highway recharging with unrestricted highway range.
- On-board rechargeable electricity storage system and a fueled propulsion power source (internal combustion engine): plug-in hybrid

For especially large EVs, such as submarines, the chemical energy of the diesel–electric can be replaced by a nuclear reactor. The nuclear reactor usually provides heat, which drives a steam turbine, which drives a generator, which is then fed to the propulsion.

A few experimental vehicles, such as some cars and a handful of aircraft use solar panels for electricity.

TABLE-1

Fuel use in vehicle designs	
Vehicle type	Fuel used
All-petroleum vehicle	Most use of petroleum
Regular hybrid electric vehicle	Less use of petroleum, but unable to be plugged in
Plug-in hybrid vehicle	Less use of petroleum, residual use of electricity
All-electric vehicle (BEV, AEV)	Exclusively uses electricity
• v • t • e	

1.1. Onboard storage

These systems are powered from an external generator plant (nearly always when stationary), and then disconnected before motion occurs, and the electricity is stored in the vehicle until needed.

-
- Full Electric Vehicles (FEV). Power storage methods include:
 - Chemical energy stored on vehicle in on-board batteries: Battery electric vehicle (BEV) typically
 - Kinetic energy storage: flywheels
 - Static energy stored on the vehicle in on-board electric double-layer capacitors

Batteries, electric double-layer capacitors and flywheel energy storage are forms of rechargeable on-board electricity storage systems. By avoiding an intermediate mechanical step, the energy conversion efficiency can be improved compared to hybrids by avoiding unnecessary energy conversions. Furthermore, electro-chemical batteries conversions are easy to reverse, allowing electrical energy to be stored in chemical form.

CHAPTER 5

TOPOLOGY OF PROPOSED EDROC

5.1 INTRODUCTION:

It is mainly composed of a six-phase PMSM, a battery, a six-phase inverter, vehicle-roof PPs, two mode switches and a digital control system. It possesses three operation modes: normal driving mode; simultaneous driving and charging mode; and dc charging mode. In normal driving mode, the switches are connected to position (nothing is connected to neutral points of six-phase PMSM). This mode is not described in detail since it has been studied in a large quantity of papers. In the following part, the other two modes are discussed and studied in depth.

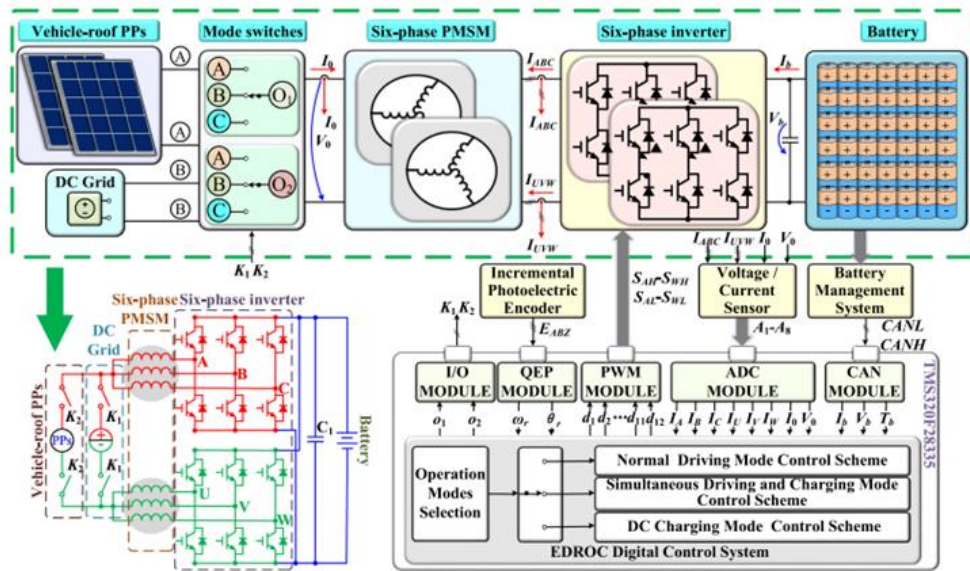


Fig. 5.1 Proposed topology of six-phase EDROC

5.2 DC CHARGING MODE:

When the EV is idle, by setting all switches at position A (powered by the vehicle-roof PPs) or B (fed by the emerging dc grid), the system will be operated in dc charging mode. For the sake of simplifying the analysis, it is assumed that the equivalent inductance and resistance of each winding of the machine are equal. Based on this, the simplified system circuit in dc charging mode can be depicted as Fig. 5.2(a), where the subscript $X \in \{A, B, C\}$ and subscript $Y \in \{U, V, W\}$. Meanwhile, SXH and SYL are kept OFF. Thus, the equivalent circuit can be further pictured as shown in Fig. 5.2(b). Notably, the circuit is analogous with two boost converters connected in series and developed to regulate charging current/voltage. Furthermore, it is worth noting that the EDROC can also be

supplied by single-phase electric grid and corresponding study has been developed. But, it is not allowed to charge from the grid and the vehicle-roof PPs at the same time.

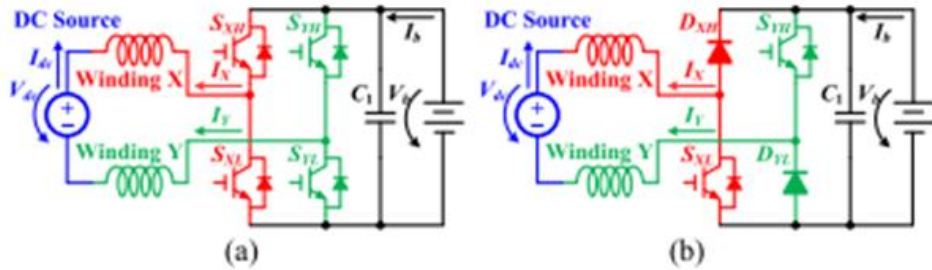


Fig. 5.2. (a) Simplified system circuit in dc charging mode. 5.2. (b) Equivalent circuit.

5.3 SIMULTANEOUS DRIVING AND CHARGING MODE:

When EV operates in driving mode and the sunlight projected onto the vehicle-roof PPs is considerably strong, by controlling all switches at position A, the system will run in simultaneous driving and charging mode, as illustrated in Fig. 3. Compared with the normal driving mode, the only difference is that the vehicle-roof PPs is connected between the two neutral points of the six-phase machine. In this mode, the power generated by the vehicle-roof PPs is responsible not only for driving but also for charging the battery as well. The principle will be discussed in Section III in considerable detail.

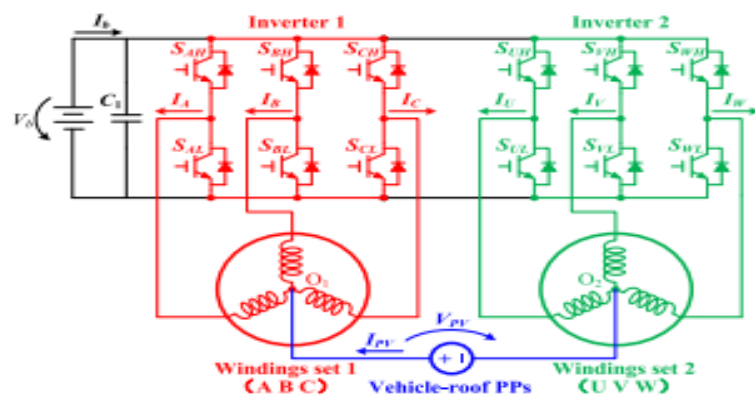


Fig. 5.3. Equivalent system circuit in simultaneous driving and charging mode

5.4 OPERATION PRINCIPLE OF EDROC:

5.4.1 OPERATION PRINCIPLE OF DC CHARGING MODE:

According to the further equivalent circuit shown in Fig. 5.2(b), it can be easily found that the system has four states [see Fig. 5.4(a)–(d)] since switches SYH and SXL can be operated in ON or OFF status. In status I, the inductances (windings X and Y) are discharged.

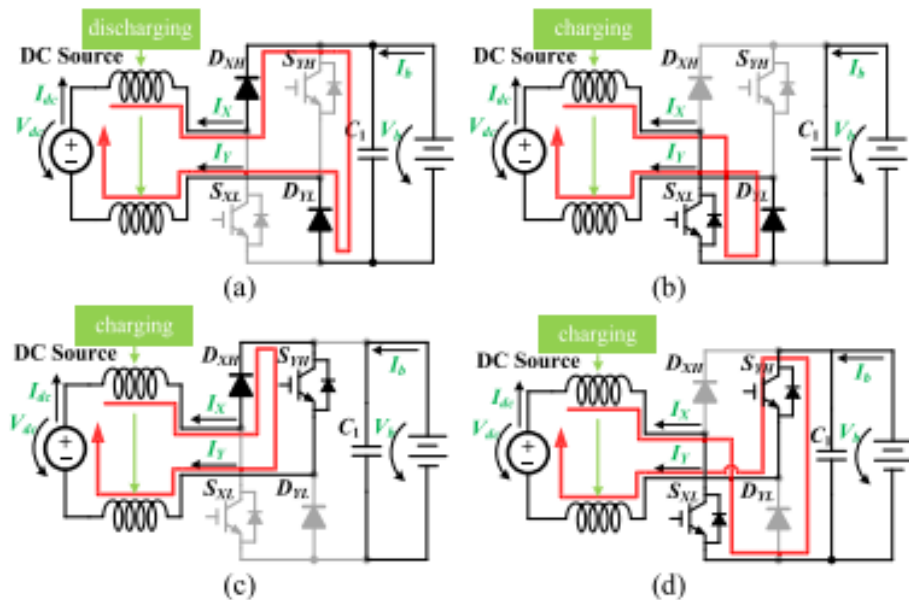


Fig. 5.4. Further equivalent circuit operation states. (a) Status I. (b) Status II. (c) Status III. (d) Status IV.

According to Kirchhoff's voltage law, the current I_{dc} pouring from dc source can be obtained as,

$$\frac{dI_{dc}}{dt} = \frac{1}{L_X + L_Y} (V_{dc} - V_b) \quad (1)$$

Where L_X and L_Y related to leakage inductance, self-inductance and mutual inductance of the machine are the equivalent inductances of windings X and Y, respectively, and it is assumed that $L_X = L_Y$ thanks to the symmetry of machine structure; V_b is battery voltage; and V_{dc} is dc source voltage. In contrast, the inductances L_X and L_Y are charged in statuses II–IV. Notably, albeit the operational circuits are diverse, I_{dc} can be expressed in the same manner for statuses II and III as

$$\frac{dI_{dc}}{dt} = \frac{1}{L_X + L_Y} V_{dc}. \quad (2)$$

Furthermore, due to the battery and the dc source charging the inductances L_X and L_Y together in status IV, the status will not be utilized. Thus, under steady-state and continuous conduction mode, (3) can be obtained according to volt-second balance principle, and by rearranging

(3), the charging voltage V_b can be denoted as (4)

$$\frac{V_{dc} - V_b}{L_X + L_Y} D_1 T_s + \frac{V_{dc}}{L_X + L_Y} (D_2 + D_3) T_s = 0 \quad (3)$$

$$V_b = \frac{1}{1 - D} V_{dc} \quad (4)$$

Where T_s is the switch period; D_1 - D_3 are the duties of statuses I-III, respectively; $D = D_2 + D_3$. Then, according to (4), there exist three control methods (see Table I) that can be implemented to regulate the charging current/voltage. Here, it needs to be noticed that the shift between SXL and SYH in method III is $0.5T_s$ and the ripples of I_{dc} in methods I and II are the same. With regard to method I and method III, the waveform of I_{dc} along with the states of SXL and SYH is drawn in Fig. 5.5, from which, it can be readily confirmed that the ripple of I_{dc} in method III is half of that in method I. Therefore, method III is of adaptation in this article

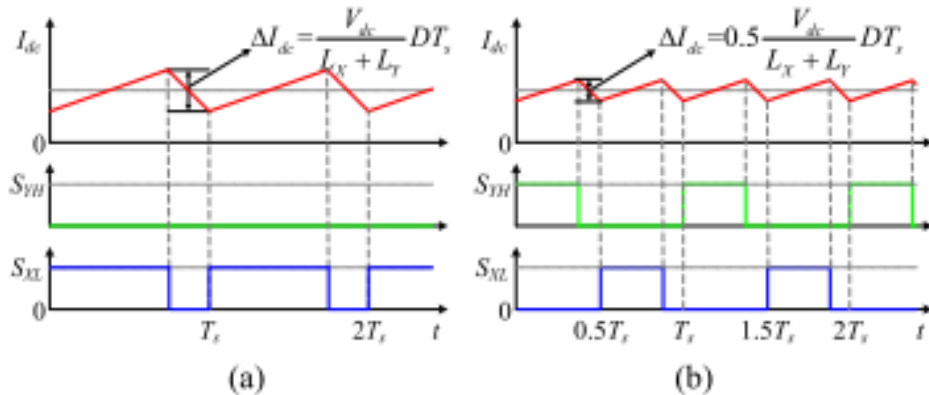


Fig. 5.5. Waveform of I_{dc} and states of SXL and SYH. (a) Method I. (b) Method III.

5.4.1.1 BUILDING THE MODEL:

Six-phase PMSM is a promising candidate for EV owing to its superiorities in terms of high efficiency, high power density, low torque ripple, and strong fault tolerance. The winding arrangement of six-phase PMSM is painted in Fig. 6, where θ is the angle between phase A and d-axis, and α is the displacement between the two three-phase windings sets. When $\alpha = 1/6 \pi$, it results in an asymmetry six-phase PMSM, namely half twelve-phase PMSM; and if $\alpha = 1/3 \pi$, it comes up with a symmetry six-phase PMSM that is explored as an example in this article. Generally, in order to simplify analysis and control, the symmetry six-phase PMSM model in the natural coordinate frame is decoupled to two 2-D orthogonal subspaces $\alpha-\beta$, $x-y$ and two zero-component axes 01 and

02 by applying decoupling matrix T1. Here, some properties of matrix T1 are as follows:

$$\mathbf{T}_1 = \frac{1}{3} \begin{bmatrix} 1 & 1/2 & -1/2 & -1 & -1/2 & 1/2 \\ 0 & \sqrt{3}/2 & \sqrt{3}/2 & 0 & -\sqrt{3}/2 & -\sqrt{3}/2 \\ 1 & -1/2 & -1/2 & 1 & -1/2 & -1/2 \\ 0 & \sqrt{3}/2 & -\sqrt{3}/2 & 0 & \sqrt{3}/2 & -\sqrt{3}/2 \\ 1/2 & -1/2 & 1/2 & -1/2 & 1/2 & -1/2 \\ 1/2 & 1/2 & 1/2 & 1/2 & 1/2 & 1/2 \end{bmatrix} \begin{array}{c|c} & \alpha \\ & \beta \\ & x \\ & y \\ & 0_1 \\ & 0_2 \end{array} \quad (5)$$

- 1) The fundamental components of the machine variables and the harmonics of order $6k \pm 1$ ($k = 1, 2, 3, \dots$) are mapped into $\alpha-\beta$ subspace. Only the variables in this subspace participate in the conversion of electromechanical energy.
- 2) The harmonics of order $3k \pm 1$ ($k=1, 3, 5, \dots$) are projected into $x-y$ subspace. These harmonics merely result in losses and therefore desire the value of zero.
- 3) The dc components and harmonics of order $3k$ ($k = 1, 3, 5, \dots$) are transferred into 01-axis. Although their roles are similar to ones in $x-y$ subspaces, they are naturally zero since the case of isolated neutral points is under consideration.
- 4) The harmonics of order $6k$ ($k = 0, 1, 2, 3, \dots$) are mapped into 02-axis. According to Kirchhoff's current law, these components are constantly zero for any six-phase machines.

By applying T1 and Park transformation TPark, three pairs of voltages can be obtained as

$$\mathbf{T}_{\text{Park}} = \begin{bmatrix} \cos \theta & \sin \theta \\ -\sin \theta & \cos \theta \end{bmatrix} \begin{bmatrix} d \\ q \end{bmatrix} \quad (6)$$

$$\begin{bmatrix} V_d \\ V_q \end{bmatrix} = R \begin{bmatrix} I_d \\ I_q \end{bmatrix} + \begin{bmatrix} L_d & 0 \\ 0 & L_q \end{bmatrix} \frac{d}{dt} \begin{bmatrix} I_d \\ I_q \end{bmatrix} + \omega_e \begin{bmatrix} -L_q I_q \\ L_d I_d + \psi_f \end{bmatrix} \quad (7)$$

$$\begin{bmatrix} V_x \\ V_y \end{bmatrix} = R \begin{bmatrix} I_x \\ I_y \end{bmatrix} + \begin{bmatrix} L_\sigma & 0 \\ 0 & L_\sigma \end{bmatrix} \frac{d}{dt} \begin{bmatrix} I_x \\ I_y \end{bmatrix} \quad (8)$$

$$\begin{bmatrix} V_{01} \\ V_{02} \end{bmatrix} = R \begin{bmatrix} I_{01} \\ I_{02} \end{bmatrix} + \begin{bmatrix} L_\sigma & 0 \\ 0 & L_\sigma \end{bmatrix} \frac{d}{dt} \begin{bmatrix} I_{01} \\ I_{02} \end{bmatrix} \quad (9)$$

Where subscripts “d” and “q” signify that the variables belong to d-q subspace; subscripts “x” and “y” represent the components of x-y subspace; subscripts “01” and “02” refer to variables in 01-axis and 02-axis, respectively; L_d , L_q , and L_σ are the d-axis inductance, q-axis inductance, and the stator leakage inductance, respectively; ω_e is the electrical angular speed, and ψ_f is the permanent magnet flux.

In the decoupled machine model, the electromagnetic torque can be expressed as

$$T_e = 3p_n I_q (I_d (L_d - L_q) + \psi_f) \quad (10)$$

Where p_n is number of pole pairs. Meanwhile, the motion equation of the machine can be depicted as

$$J \frac{d\omega_m}{dt} = T_e - T_L \quad (11)$$

Where ω_m is the mechanical angular speed; J is the inertia moment referred to the rotor; and T_L is the load torque.

5.4.2 OPERATION PRINCIPLE OF SIMULTANEOUS DRIVING & CHARGING MODE:

In this mode, the vehicle-roof PPs is connected between the neutral points of machine as shown in Fig. 3. Based on the law of conservation of energy and ignoring the power loss, the following expression is obtained

$$\begin{aligned} P_b &= P_m - P_{PV} \\ P_b &= V_b I_b, P_m = k_m n_m T_e, P_{PV} = V_{PV} I_{PV} \end{aligned} \quad (12)$$

Where P_b is battery output power, and the battery is discharged (or charged) if $P_b >$ (or $<$) 0; V_{PV} denotes vehicle-roof PPs voltage; and I_{PV} represents the vehicle-roof PPs output current. Besides, from (10) and (11), it is worth noticing that T_e and n_m can be controlled by adjusting I_d and I_q ; therefore, P_m can be readily regulated in the same manner. In the meantime, P_{PV} is practically dependent on I_{PV} which can be adjusted by 01-axis current I_{01} . Furthermore, as shown in Fig. 7, from the function perspective, the six-phase system can be regarded as a machine drive inverter function module controlling dq-axes components together with a dc/dc function module regulating 01-axis component to realize the MPPT purpose. The dc components and harmonics of order $3k$ ($k = 1, 3, 5, \dots$) are transferred into 01-axis. Although their roles are similar to ones in x–y subspaces, they are naturally zero since the case of isolated neutral points is under consideration.

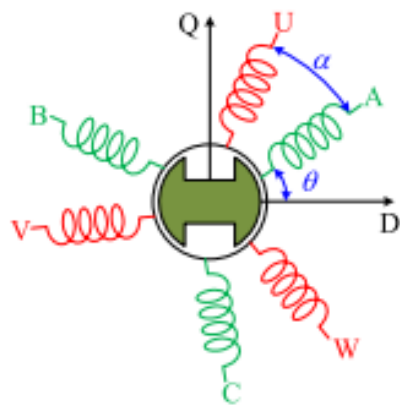


Fig. 5.6. Winding arrangement of six-phase PMSM

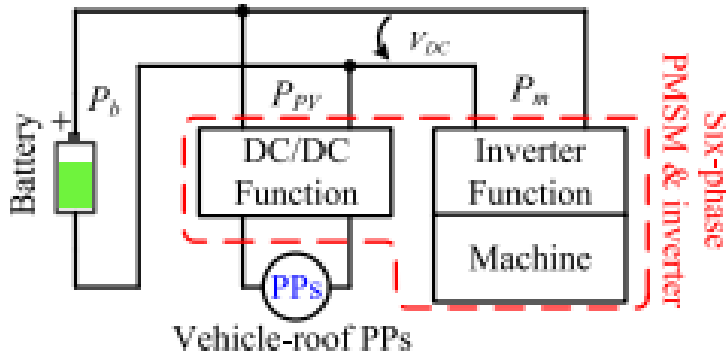


Fig.5. 7. Equivalent system structure in simultaneous driving and charging mode.

The two modules share the circuit and connected to the battery in parallel, but they are irrelevant for each other thanks to the decoupling between the O1-axis and dq-axes components. It should be mentioned that the machine drive inverter function module only plays the load role to convert the electric energy to the mechanical energy; the dc/dc function module only serves as a source, and its power generation is determined by the solar irradiation; besides, the battery can function as both a load or a source, contingent on the power generation of PPs. In addition, it should be mentioned that the dc/dc function module output voltage is equal to the dc-bus voltage VDC.

On this basis, the power distribution schematic presentation can be shown in Fig. 8, where the green arrow denotes the power flow in the system. In case PPV the dc-bus voltage VDC will be slightly lower than the battery open-circuit voltage Vbo and the battery will output energy. As such, the system is powered by two sources, namely the battery and the vehicle-roof PPs. Otherwise, VDC will be slightly higher than Vbo, so the battery will be charged. In this manner, only the vehicle-roof

PPs provide energy to cover the drive requirement, and the remaining energy is transformed into the battery. Hence, Pb can be changed through the control of I01, in conjunction with the regulation of Id and Iq. And the operation is feasible owing to the decoupling relationship between Id, Iq, and I01. In summary, the operation in the mode can be implemented as:

- (1) Regulate Id and Iq to track the desired speed;
- (2) Control Ix and Iy to zero in order to decrease losses;
- (3) Adjust I01 according to the MPPT of the vehicle-roof PPs for the minimization of Pb.

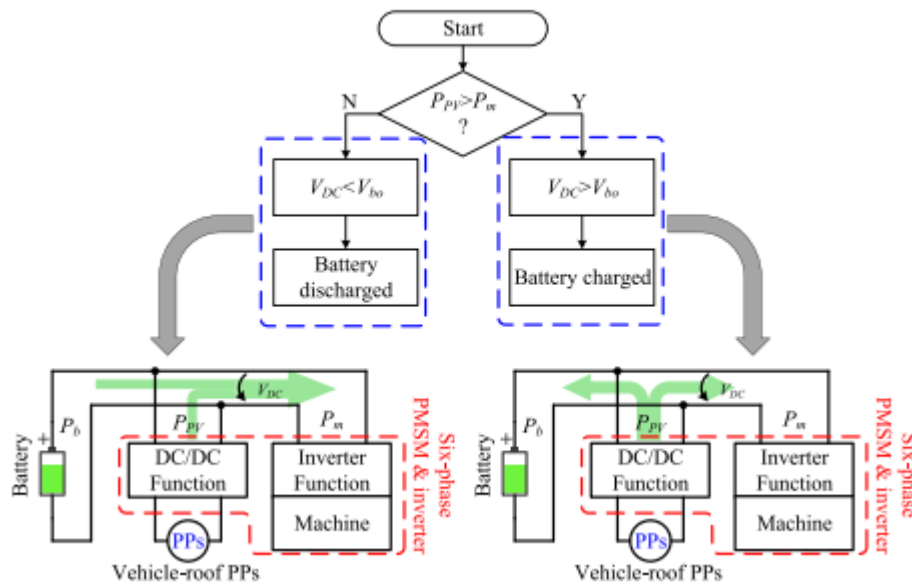


Fig.5. 8. Power distribution in simultaneous driving and charging mode.

5.5 NECESSARY CONDITIONS FOR THE EDROC:

To ensure safe and stable operation of the charger, the necessary conditions are discussed hereafter. In the dc charging mode, the function between V_b and V_{dc} is represented as . Considering $0 \leq D < 1$.

Furthermore, in this mode, I_{dc} is sum of currents flowing windings A, B, and C (or U, V, and W) so that

$$V_{dc} \leq V_b. \quad (13)$$

I_{dc} is limited as

$$I_{dc} \leq 3I_{P\max,rms} \quad (14)$$

where $I_{P\max,rms}$ is the maximum allowable current flowing the phase winding. In the simultaneous driving and charging mode, can be rewritten as

Where V_{ABC} and V_{UVW} are, respectively, the common mode voltages for the first set of windings (ABC) and the second set of windings (UVW) and both values are in the range of $-0.5V_b$ to $0.5V_b$. In addition, in steady state, $dI_{01}/dt = 0$ and RI_{01} is negligible because R is quite small. Hence, V_{PV} is limited as

$$\frac{V_{ABC}-V_{UVW}}{2} = \frac{V_{PV}}{2} + RI_{01} + L_\sigma \frac{dI_{01}}{dt} \quad (15)$$

$$0 < V_{PV} < V_b. \quad (16)$$

Besides, the current I_{01} realizing the power transfer between battery and vehicle-roof PPs is imposed on the torque producing currents I_q and I_d . Thus, the limitation of machine current is derived as and corresponding waveforms of allowable q-axis current for different operating points are illustrated. It can be noticed that the maximum allowable q-axis current reduces with increasing of I_{01} . That means that the maximum allowable electromagnetic torque will decrease in simultaneous driving and charging mode

$$\sqrt{I_{01}^2 + \frac{4I_{01}\sqrt{I_q^2 + I_d^2}}{\pi} + \frac{1}{2}(I_q^2 + I_d^2)} \leq I_{P\max,rms}. \quad (17)$$

In addition, the battery voltage constrains the inverter output voltage. Omitting the possible over-modulation, the maximum inverter output voltage is $V_{P,\max} = 0.5V_b$ under pulse width modulation (PWM). For the sake of simplifying analysis, assuming that $I_d = I_x = I_y = 0$, the inverter voltage components V_d , V_q and V_{01} are limited as

$$\sqrt{V_d^2 + V_q^2} + V_{01} \leq V_{P,\max} \quad (18)$$

Where it needs to be noted that $V_{01} = 0.5(V_{ABC}-V_{UVW})$. Ignoring the wingding resistance and substituting (7) into (18) in steady-state, it yields

$$(\omega_e L_q I_q)^2 + (\omega_e \psi_f)^2 \leq \left(V_{P,\max} - \frac{1}{2} V_{PV} \right)^2. \quad (19)$$

According to (19), when $L_q = 2$ mH, $\psi_f = 0.042$ Wb, $p_n = 5$ and $V_{P,\max} = 75$ V, the curve of the maximum allowable of VPV for different operation points is draw. It can be easily observed that the maximum allowable speed n_m decreases with the increase of I_q and V_{PV} . In summary, the machine driving performances (the maximum allowable electromagnetic torque and the maximum allowable speed) of the system will decline slightly in the simultaneous driving and charging mode. Hence, VPV needs to be dynamically clipped during extreme acceleration and high-speed events. In this mode, instead of the measured values, the setting values of I_{01} , I_q , I_d , and ω_e will be used in (17) and (19) to observe the now or next operating status of the system. When (17) and (19) are not satisfied, the vehicle-roof PPs will be removed. Otherwise, the vehicle-roof PPs will be connected. Fortunately, clipping action is expected to be rare, since the required minimum driving voltage in the period of travelling appears to be significantly smaller than battery voltage and the periods of extreme acceleration and high-speed are infrequent.

5.6 MANAGING SIGNALS AND PARAMETERS:

5.6.1 MPPT AND CONSTANT VOLTAGE/CURRENT CHARGING CONTROL:

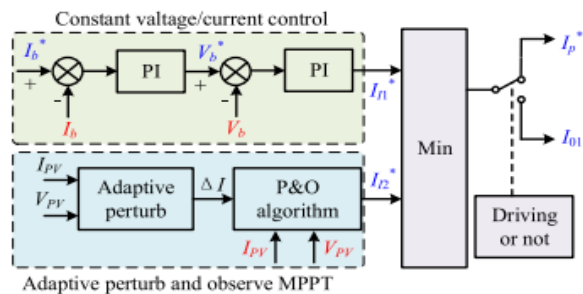


Fig. 5.9. MPPT and constant voltage/current charging control block diagram.

As shown in Fig. 5.9, the control scheme mainly consists of two portions: constant voltage/current charging control and adaptive perturb and observe (P&O) MPPT control. For the former part, two PI controllers connected in series are set up. The first PI controller is employed to track the desired charging current I_b^* , and the second one is used to regulate charging voltage V_b . In particular, if the charging voltage reference V_b^* generated by the first PI controller is less than the maximum charging voltage of battery V_{b_max} , constant current charging will be implemented; otherwise, constant voltage charging will be carried out, which is actually corresponding to the case that the first PI controller is in state of saturation. Regarding the latter one, the value of perturb current

ΔI is determined via the adaptive perturb generation module. Then, the desired output current of vehicle-roof PPs is obtained through the P&O algorithm. The detailed design process of the MPPT has been studied in [28]. The smaller one between two output values of two portions is chosen as the desired input current. Finally, according to the state of EV, the desired input current is used as either the 01-axis reference current I_{01*} or the winding reference current I_{P*} . Here, it should be noted that the output value of constant voltage/current charging control is used as winding reference current I_{P*} when the system is operated in dc charging mode and emerging dc grid is employed.

5.6.1.1 DC CHARGING MODE:

On the basis of the principle of magnetic energy and magnetic co-energy theory [29]–[31], the average electromagnetic torque T_e produced by the six phase PMSM can be derived as

$$T_e = P_n \left(\mathbf{I}^T \psi_f \frac{\partial \xi}{\partial \theta_e} + \frac{1}{2} \mathbf{I} \frac{\partial \mathbf{L}}{\partial \theta_e} \mathbf{I}^T \right) \quad (20)$$

Where $\xi = [\cos(\theta_e) \cos(\theta_e - \pi/3) \dots \cos(\theta_e - 5\pi/3)]$; \mathbf{I} is the phase currents matrix; \mathbf{L} is the motor inductance matrix. This equation suggests the electromagnetic torque can be calculated in terms of the rotor position as long as \mathbf{I}, \mathbf{L} , and ξ are measured or identified. Particularly, when six windings carry the same currents, namely $I_A = I_B = I_C = I_U = I_V = I_W$, zero electromagnetic torque production can be ensured, regardless of the rotor position. Therefore, as depicted in Fig. 5.10, the desired currents of six windings be identical and six PI controllers are applied to regulate corresponding winding current. Meanwhile, as discussed in Section III-A, the duties of SAL and SUH (SVH, or SWH) both contribute to I_A , possibly resulting in huge difference between d_A and d_U . Hence, the average duty strategy is adopted to follow: calculate the average d_{m1} of duties d_A , d_B , and d_C and the average d_{m2} of duties d_U , d_V , and d_W ; calculate the average d_m of d_{m1} and d_{m2} ; and obtain the duties d_x ($x = 4, 5, \dots, 9$) based on

$$\begin{cases} d_4 = d_A + d_m - d_{m1} \\ d_5 = d_B + d_m - d_{m1} \\ d_6 = d_C + d_m - d_{m1} \\ d_7 = d_U + d_m - d_{m2} \\ d_8 = d_V + d_m - d_{m2} \\ d_9 = d_W + d_m - d_{m2}. \end{cases} \quad (21)$$

Finally, the gate signals are generated by two PWM modules, in which the phase shift between two carriers is $0.5T_s$ (T_s is carrier cycle and $T_s = 0.1$ ms) to decrease the phase currents switching ripple.

5.6.1.2 SIMULTANEOUS CHARGING AND DRIVING MODE:

The control scheme is based on a conventional solution of current control using simple PI controllers, as presented. Five current PI controllers are required since there are five independent current components mapped into two decoupled reference frames accompanied with one zero axis as: the main reference frame d–q, in which torque production of the machine is controlled; the harmonic reference frame x–y, where current harmonics are controlled; and zero axis 01, where vehicle-roof PPs output current is controlled. First, a speed PI controller is employed to track the desired speed n^* , in tandem with the desired q-axis current I_{q*} generation. Next, I_{d*} is set to zero and then the current components in the d–q frame are adjusted by two current PI controllers. Secondly, the currents of x–y frame desire zero since they do not contribute to conversion of electromechanical energy, and thus the current components of the x–y frame are regulated to zero via x–y frame PI controllers. Then, the PPs output current is controlled by 01-axis current PI controller. After that, to eliminate the cross-coupling effects in the stator voltage (7), the following decoupling voltages should be under consideration

$$\begin{cases} V_d^{\text{decouple}} = -\omega_e L_q I_q \\ V_q^{\text{decouple}} = \omega_e (L_d I_d + \psi_f). \end{cases} \quad (22)$$

Finally, the gate signals are obtained by two PWM modules and two negation modules.

CHAPTER 6

SIMULATION RESULTS

6.1 CASE-01 – DC CHARGING MODE:

Firstly, dc charging mode is conducted. As fore-mentioned, switches SAH, SBH, SCH, SUL, SVL, and SWL are always kept OFF, as shown while the other switches operate at 10 kHz. The waveforms of charging current, charging voltage, and currents flowing through machine's phase A and phase B under constant current charging mode. The dc power supply connected between two neutral points of machine is set to 95V. It can be observed that the charging current I_b follows its desired value, with a constant charging voltage 148v.

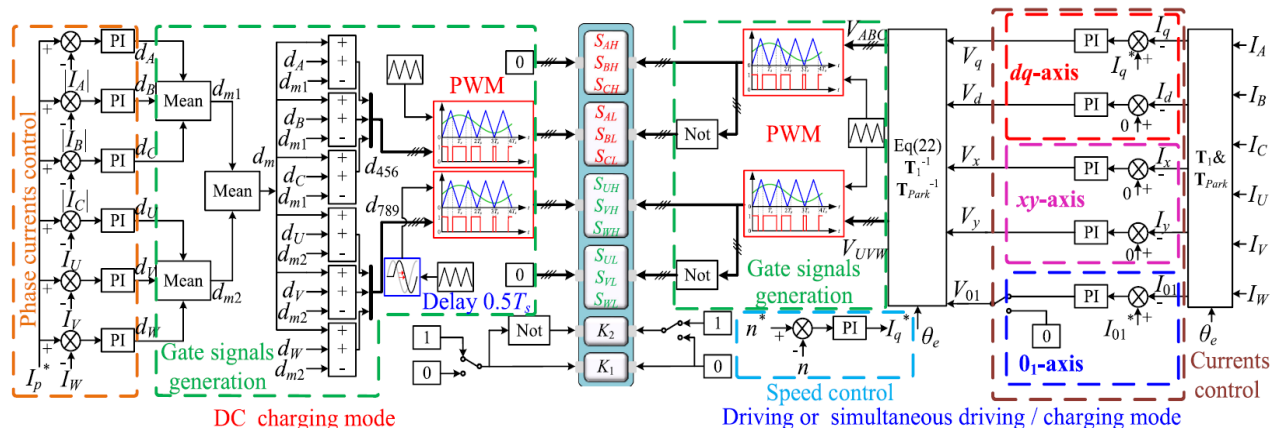


Fig. 6.1. control diagram

The same amplitudes of phase currents are obtained, ensuring zero electromagnetic torque generation. Besides, the phase current ripple is around 1.7 A, while the charging current ripple is negligible, which shows a key characteristic for battery charging operation. To verify the dynamic performance under dc charging mode, the charging current is varied in a step manner from 5 to 10 A, as presented. Excellent charging current-tracking performance can be observed, together with the constant charging voltage. The phase currents are always the same throughout the dynamic adjustment process, preventing the torque generation during response process.

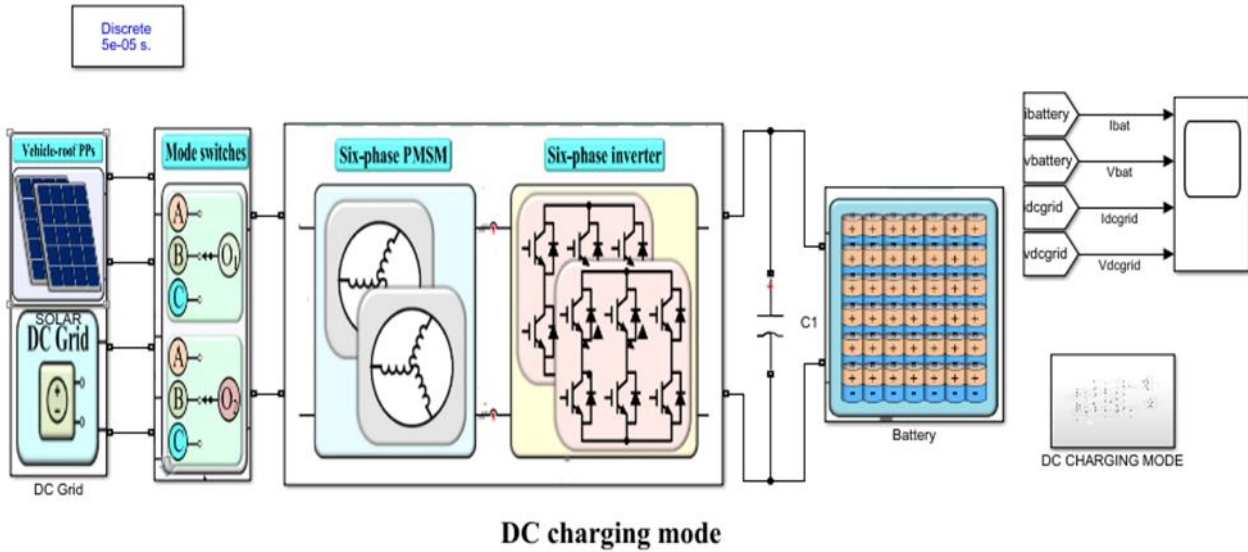


Fig. 6.2. Schematic diagram

6.1.1 CONTROLLING UNIT:

Then, in order to verify the effectiveness and superiority of the six-PI control method, the single PI control method is conducted in the same condition. When the phase currents are controlled by one PI controller, the A phase current IA is unequal to the phase current IB under the nonidentical equivalent impedances of machine phase windings owing to the anisotropy of the machine. But, when the phase currents are independent controlled by six PI controllers, the A phase current IA is same as the phase current IB. Finally, the average duty strategy

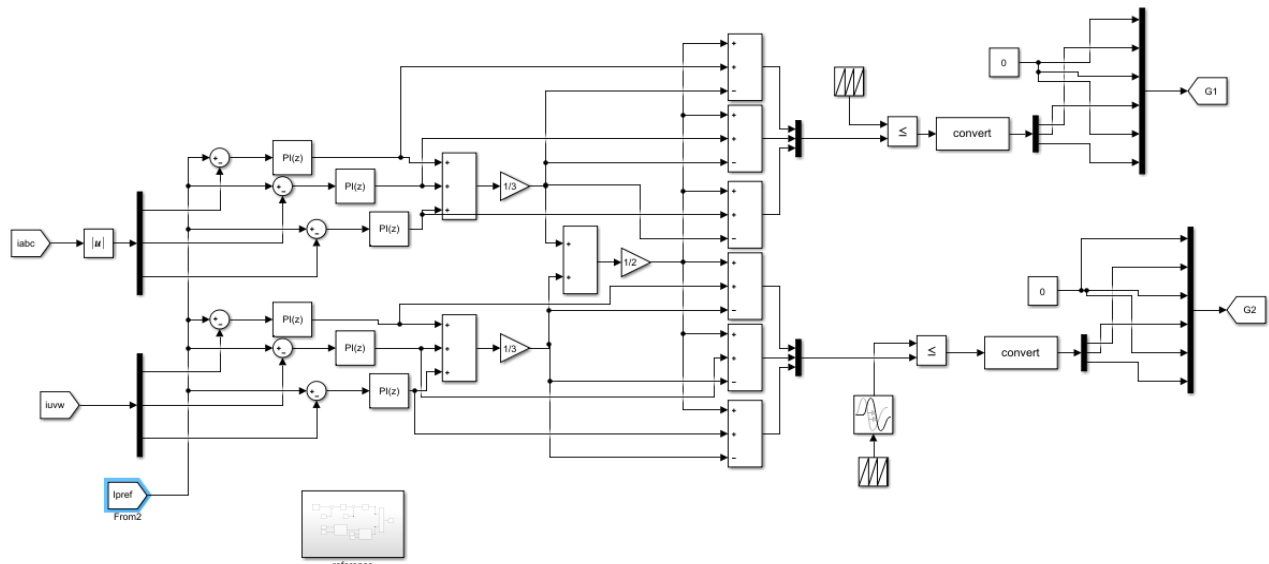


Fig. 6.3. Controlling part

6.1.2 REFERENCE CURRENT:

Finally, the average duty strategy is evaluated under the condition of desired charging current of 10 A, as shown. The average duty strategy is not activated, in which case, the signal to drive SUH is approximately of zero duty. As observed, the magnitude of current ripple (for both IA and IU) is about 3A. Thereafter, the average duty strategy is employed simultaneously. Two switching signals are of the same duty, and a phase shift between them is one half of the switching period. Meanwhile, a rather improvement in terms of the magnitude of current ripple can be observed (from approximately 3 to 1.7 A). The amplitudes of IA and IU are not identical as observed. In addition, the output current of battery is approximately -1.2 A, which means that the battery is charged. The FFT results of IA in the simultaneous driving and charging mode and the normal driving mode are depicted. The total harmonic distortion (THD) of phase current in the simultaneous driving and charging mode is about 5.95%, which is higher than that in normal driving mode (3.87%). This increase is especially associated with second-order harmonic as a result of the unequal impedances of stator windings.

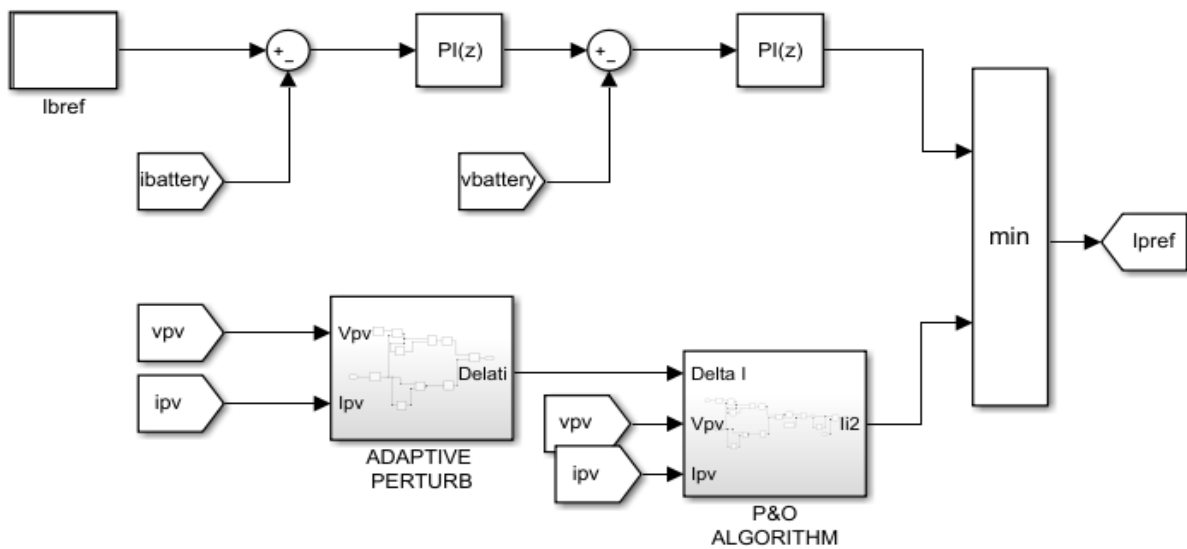


Fig. 6.4. Reference current

6.1.3 SOURCE CODE [Parameters]:

```
%% parameters pv side
%% six phase pmsm
prasi=2e3;
time=[0 0.5];
torquel=[4.5 4.5];
wrated=2000;
np=5;
R=0.3;
ld=5.56e-3;
lq=7e-3;
oaxis=0.125e-3;
rphas=0.3;
fluxsta=0.042;
ja=0.02;
%% battery side
ratbat=50;
vba=144;
imaxchar=25;
imaxdisc=25;
```

6.1.3.1 MODE – 0:

Only DC grid is connected.

i.e., $K=0$; I_{pv} (current supplied from PV array) is approximately equal to zero

$I_{bref}=[5 \ 5]$

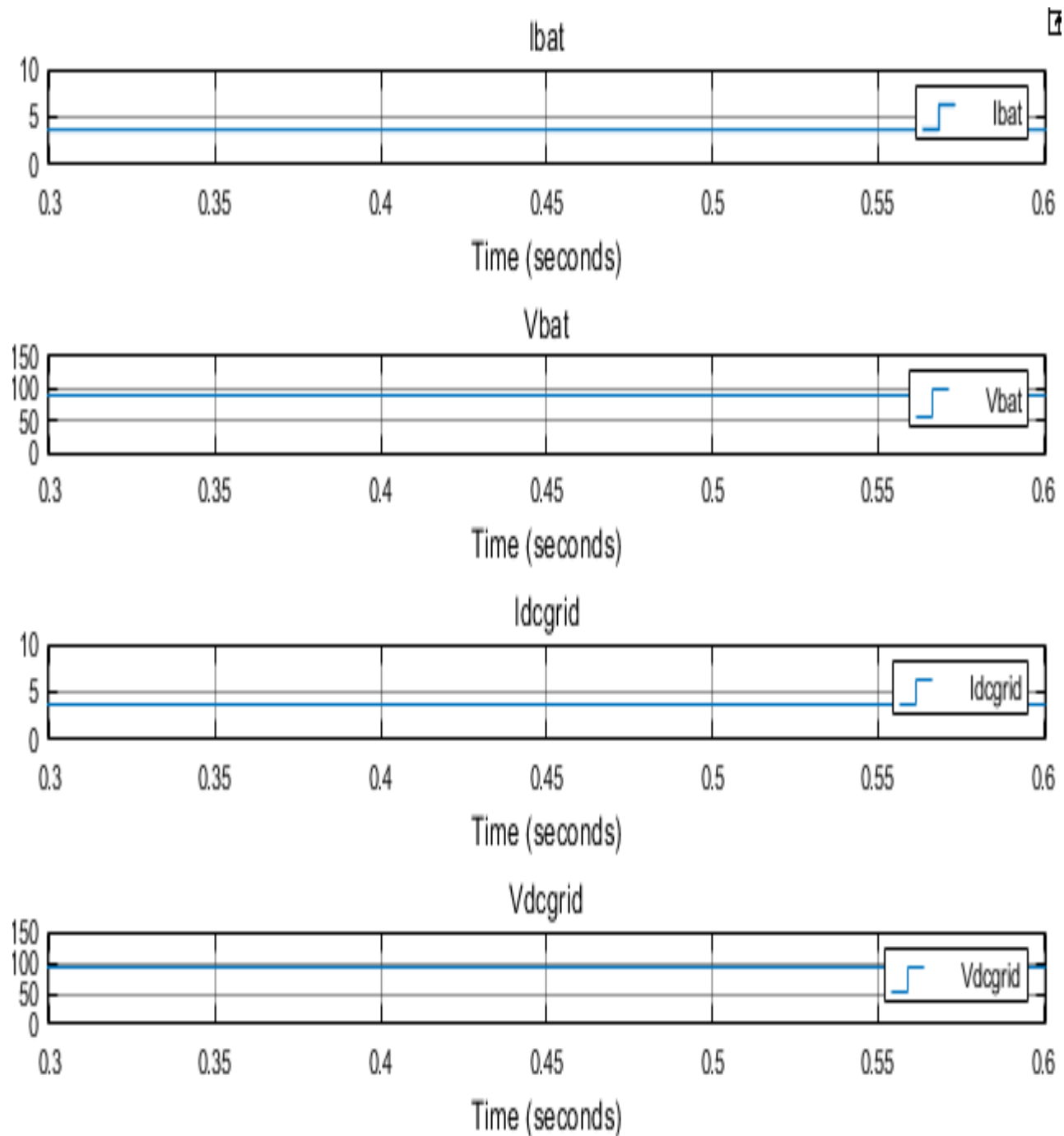


Fig. 6.5. steady state connected to grid

Only solar is connected.

i.e., $K=1$; I_{bet} (current supplied from grid) is approximately equal to zero

$I_{bref}=[5 \ 10 \ 10]$.

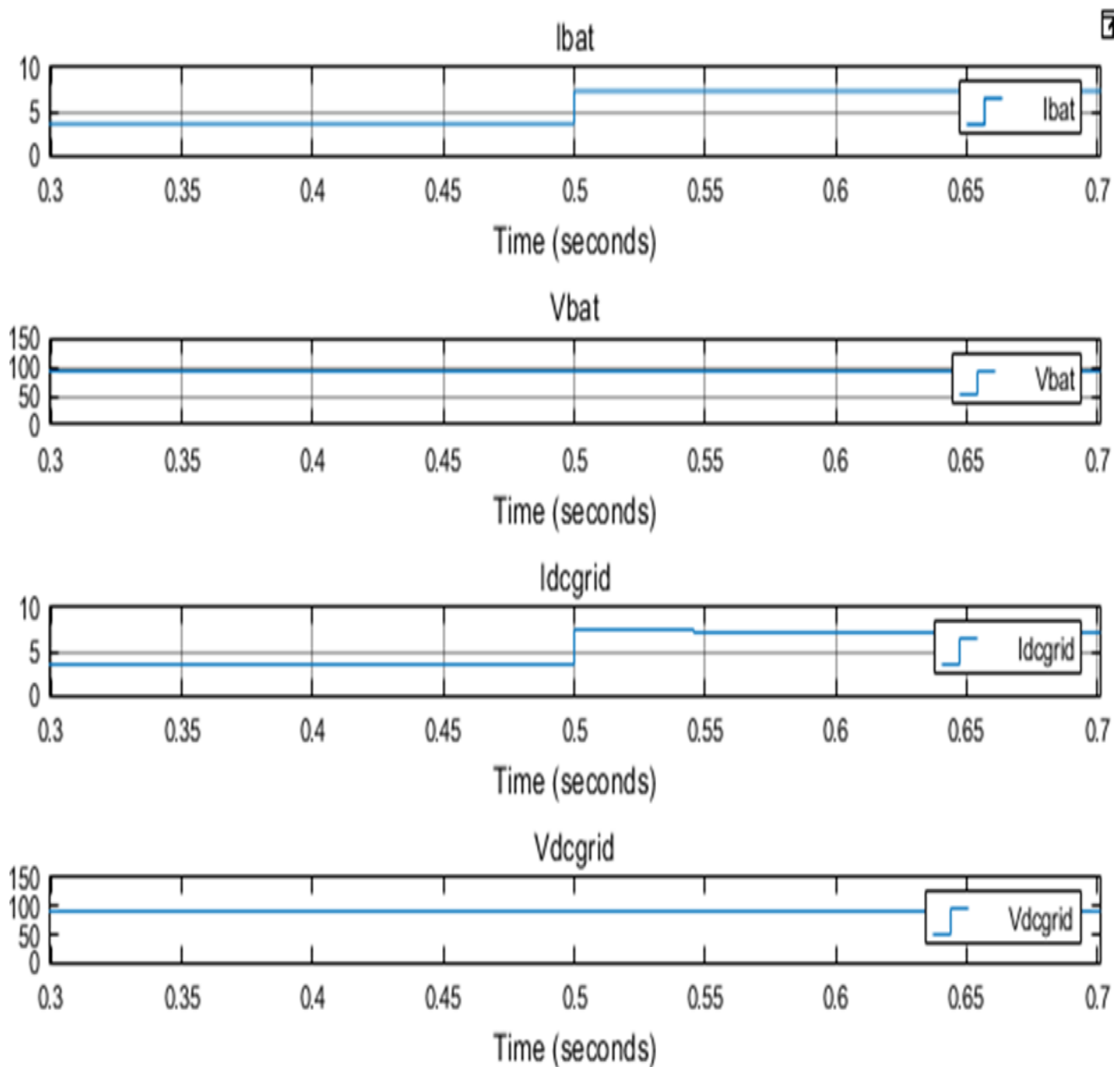


Fig. 6.6. dynamic state connected to solar

6.1.3.2 MODE – 1:

Only DC grid is connected.

i.e., $K=0$; I_{pv} (current produced from PV array) is approximately equal to zero

$I_{bref}=[5 \ 5 \ 5]$.

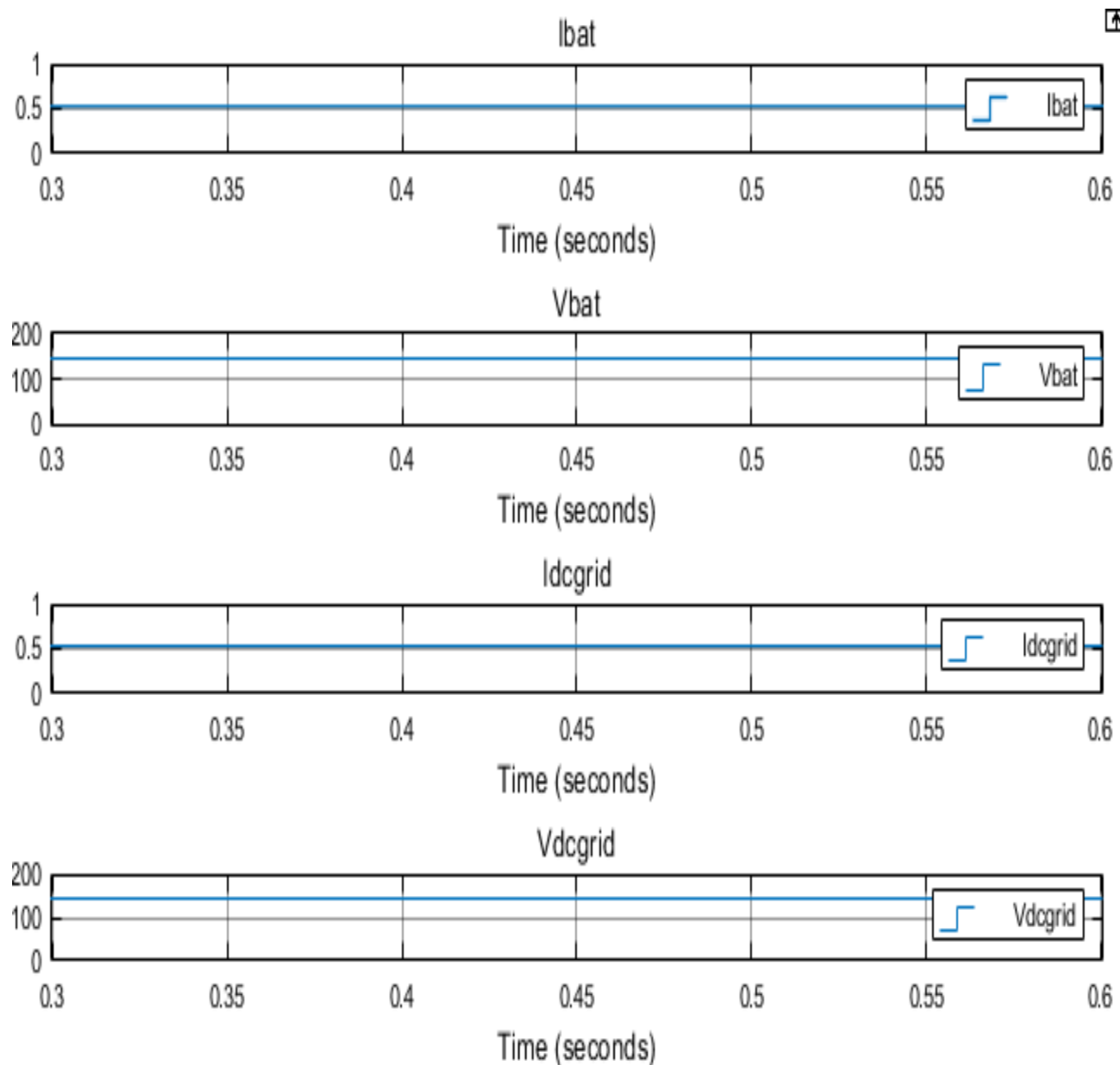


Fig.6.7. steady state connected to grid

Only solar is connected.

i.e., $K=1$; I_{bet} (current supplied from grid) is approximately equal to zero

$I_{bref}=[5 \ 10 \ 10]$.

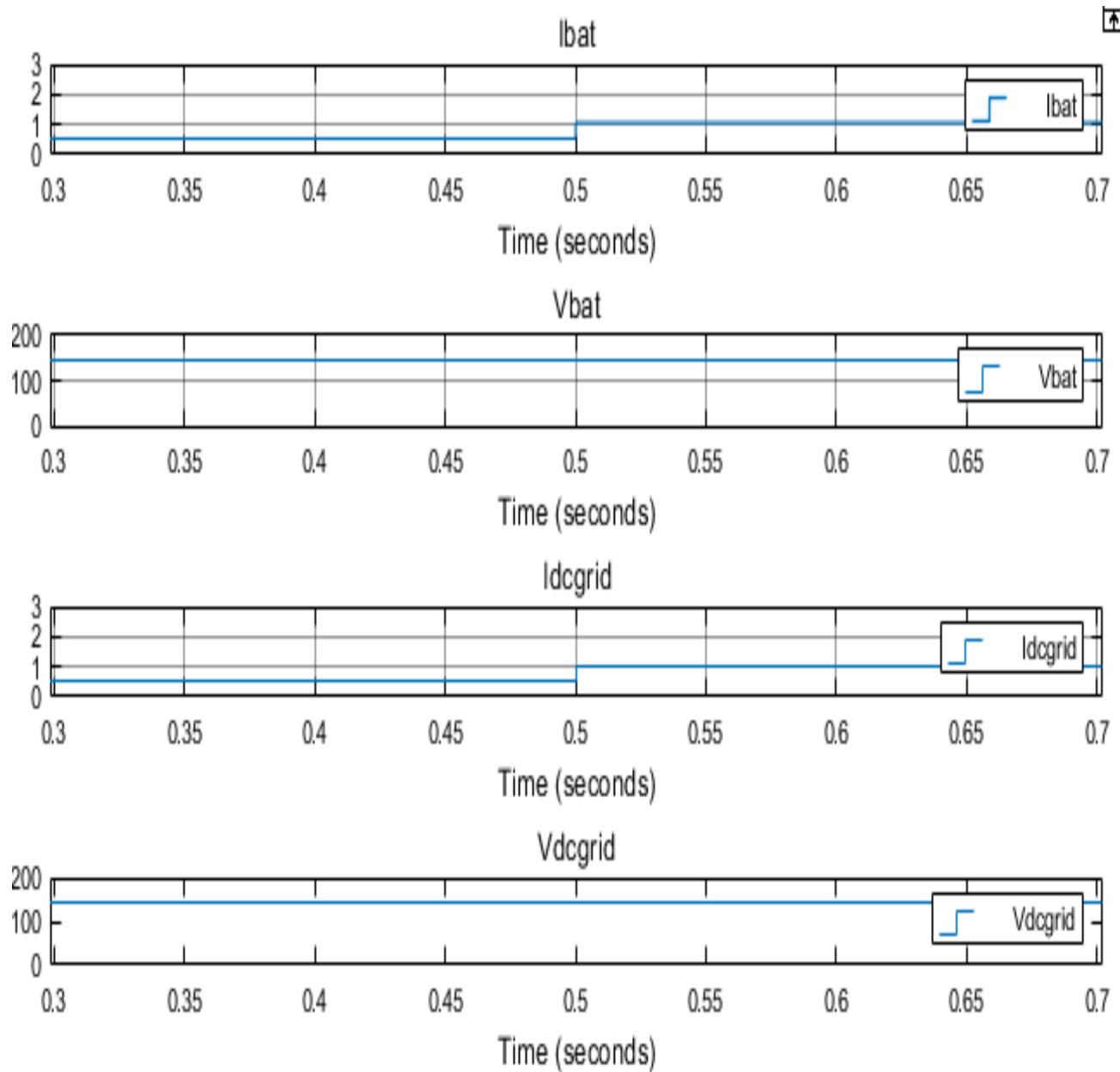


Fig. 6.8. dynamic state connected to solar

6.2 CASE – 02- SIMULTANEOUS CHARGING AND DRIVING MODE:

6.2.1 LOAD AND SPEED CONSTANT:

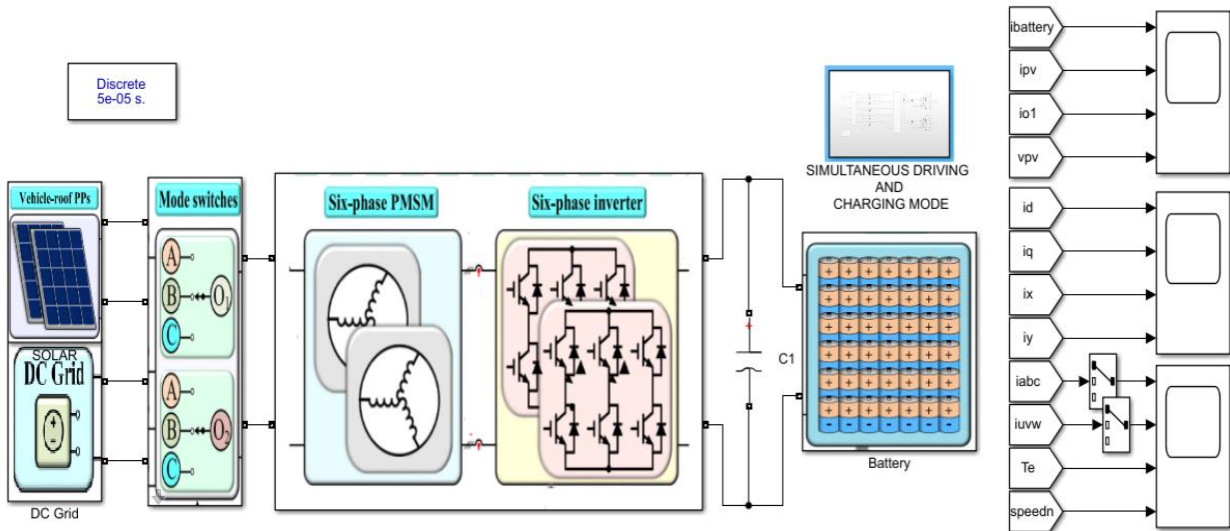


Fig.6.9. Schematic diagram

The simultaneous drive and charging mode is conducted according to the control algorithm. In this mode, the PPs are in the condition of $1050\text{W}/\text{m}^2 18^\circ\text{C}$. Depicts the steady-state performance under the desired speed of 500 r/min in conjunction with 4.5 N-m load. It can be observed that the phase currents are extremely sinusoidal. Meanwhile, the d-, q-, x-, y-axes currents, speed as well as output torque of the machine are constant. Besides, because of the injection of 01-axis current causing opposite effects on two sets of three-phase windings the amplitudes of IA and IU are not identical as observed. In addition, the output current of battery is approximately -1.2 A , which means that the battery is charged. The FFT results of IA in the simultaneous driving and charging mode and the normal driving mode are depicted. The total harmonic distortion (THD) of phase current in the simultaneous driving and charging mode is about 5.95% , which is higher than that in normal driving mode (3.87%). This increase is especially associated with second-order harmonic as a result of the unequal impedances of stator windings. The dynamic responses are illustrated in Figs. 18 and 19, which are pertinent to speed step-change from 1000 to 500 r/min and load step-change from 8 to 4.5 N-m , respectively.

6.2.2 CONTROLLING UNIT:

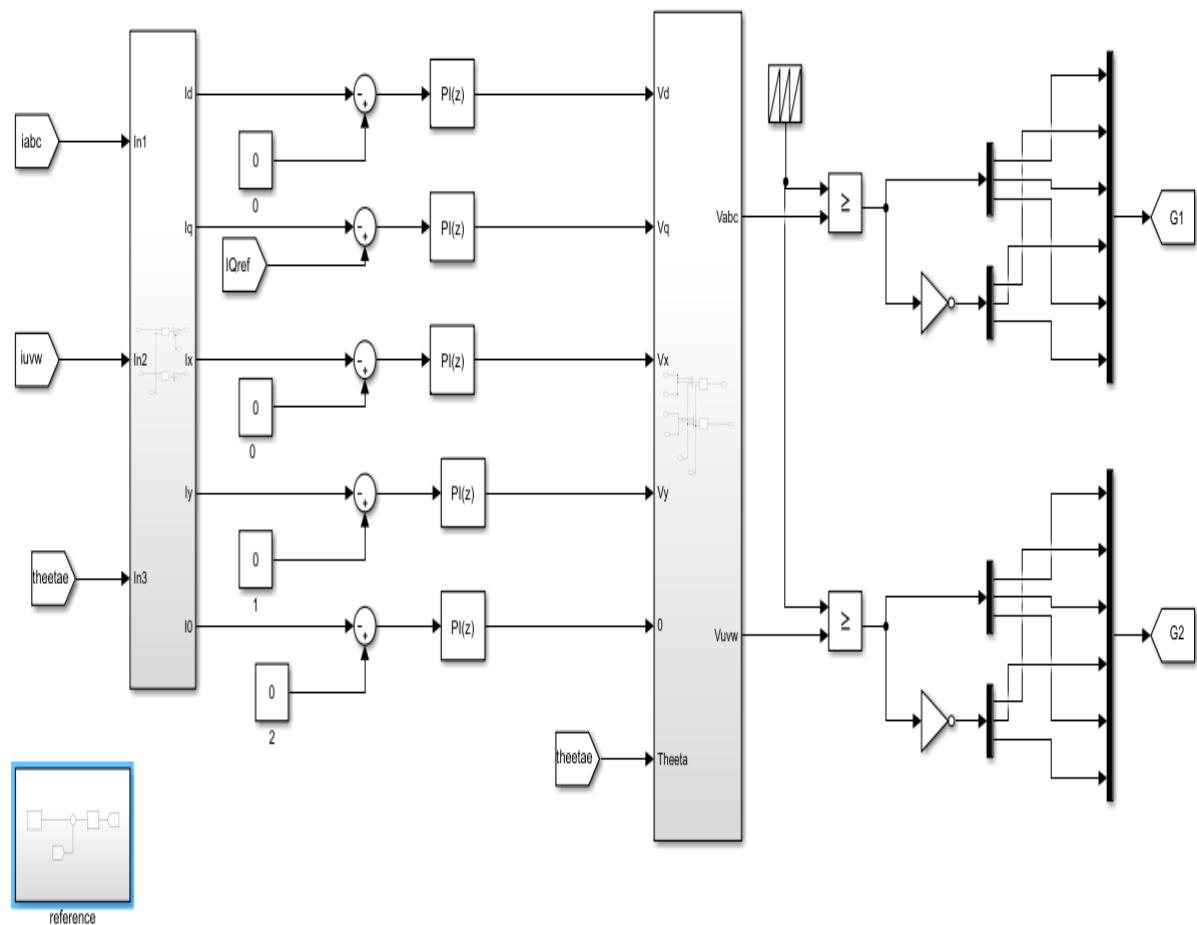


Fig.6.10. Controlling part

6.2.3 SPEED CONTROL UNIT:

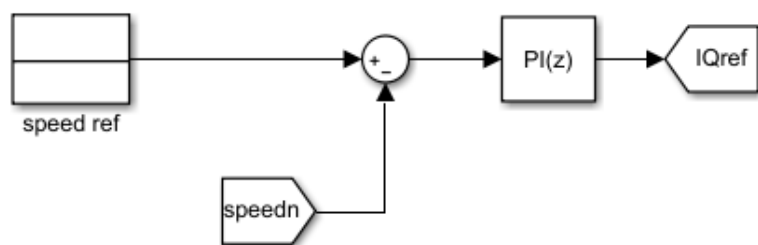


Fig.6.11. Speed controller

6.2.4 SOURCE CODE [Dynamic load]:

```
%% parameters pv side
```

```
%% six phase pmsm
```

```
prasi=2e3;
```

```
time=[0 0.5];
```

```
torquel=[8 4.5];
```

```
wrated=2000;
```

```
np=5;
```

```
R=0.3;
```

```
ld=5.56e-3;
```

```
lq=7e-3;
```

```
oaxis=0.125e-3;
```

```
rphas=0.3;
```

```
fluxsta=0.042;
```

```
ja=0.02;
```

```
%% battery side
```

```
ratbat=50;
```

```
vba=144;
```

```
imaxchar=25;
```

```
imaxdisc=25;
```

6.2.4.1 BOTH LOAD AND SPEED ARE CONSTANT:

Output current and voltage of solar PV array,
battery current and 01-axis current outputs can be as follow:

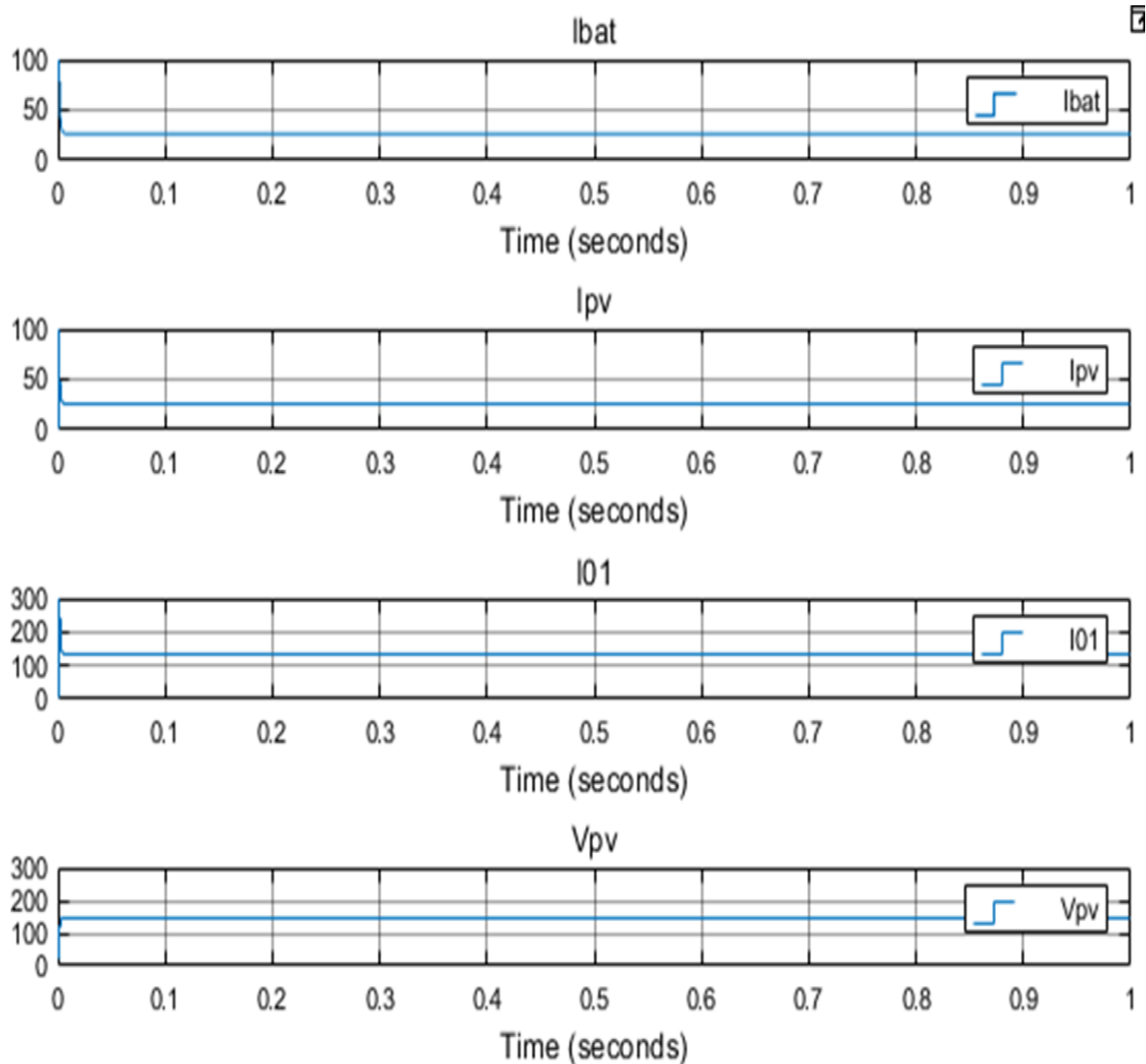


fig.6.12. PPs output current and voltage, battery current and 01-axis current.

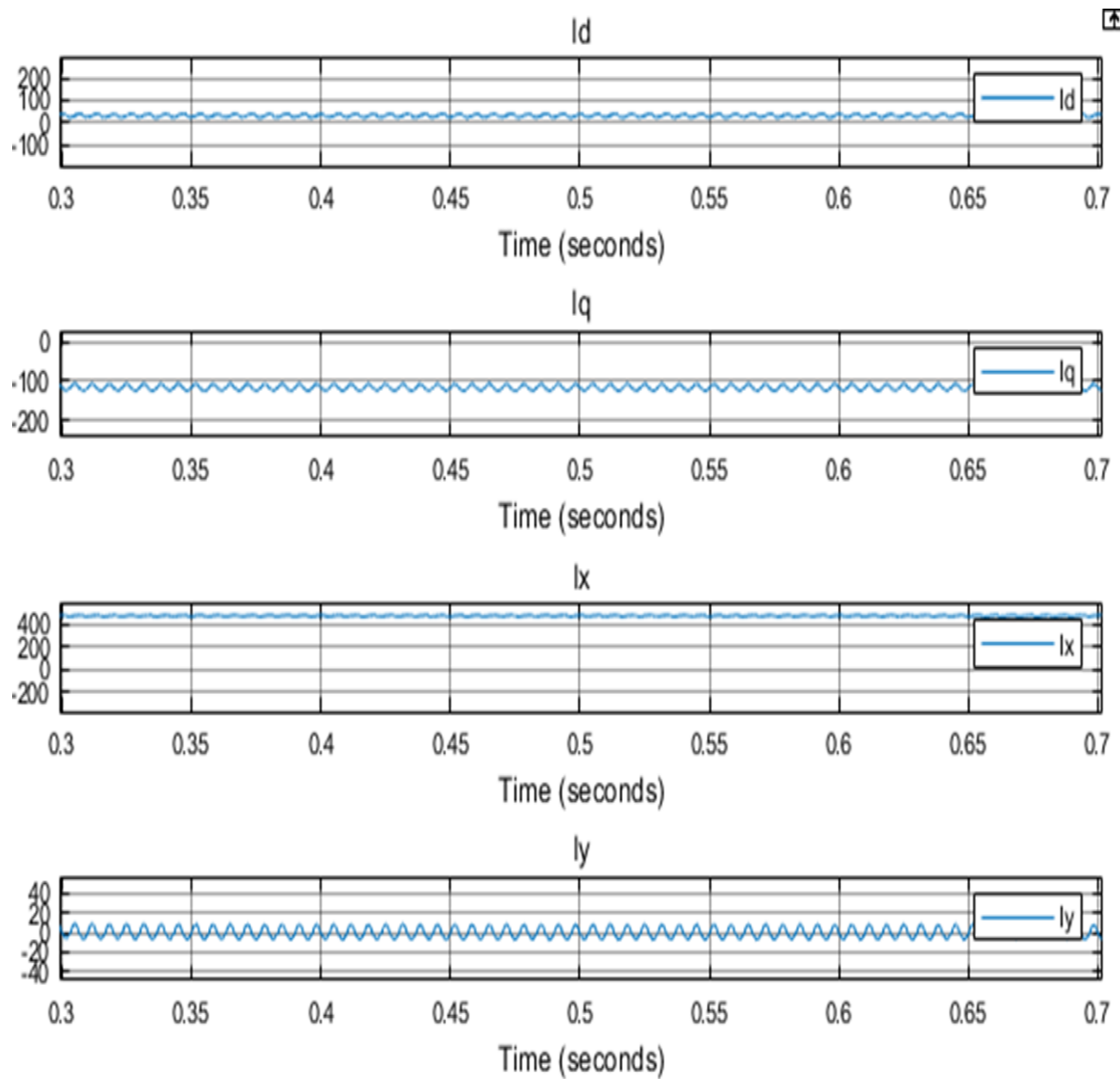


Fig.6.13. Currents in d-axis, q-axis, x-axis, and y-axis.

The load and speed remains constant
The phase currents I_a , I_u , remains constant
Reference speed=[500 500 500]

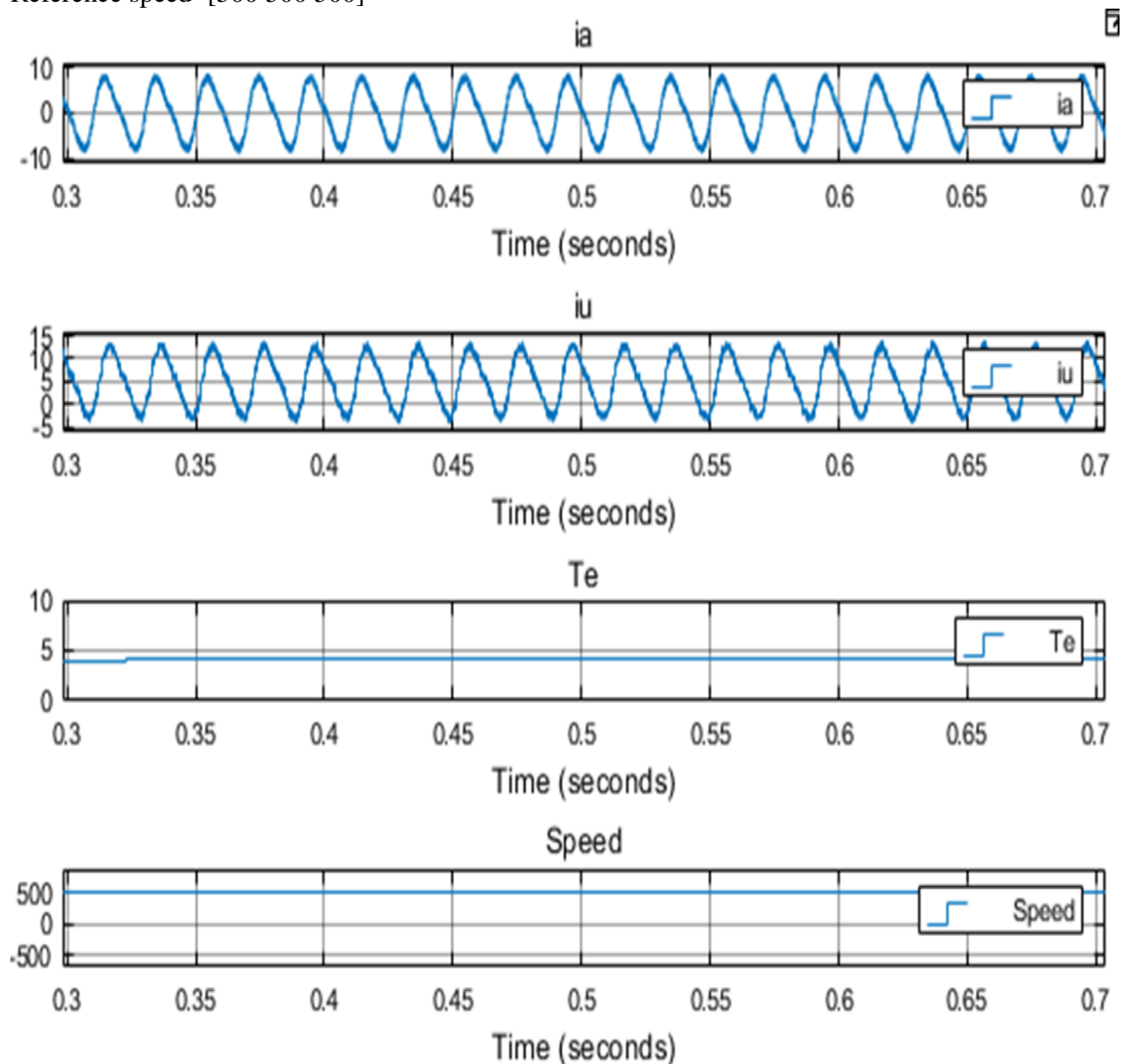


Fig.6.14. Currents in phase A and U, speed, and output torque

6.2.4.2 LOAD IS VARIABLE AND SPEED IS CONSTANT:

The load is changed at 0.5 amplitude. Also load parameters changes as shown in source code.
The phase currents I_a , I_u and torque but speed remains constant
Reference speed=[500 250 250]

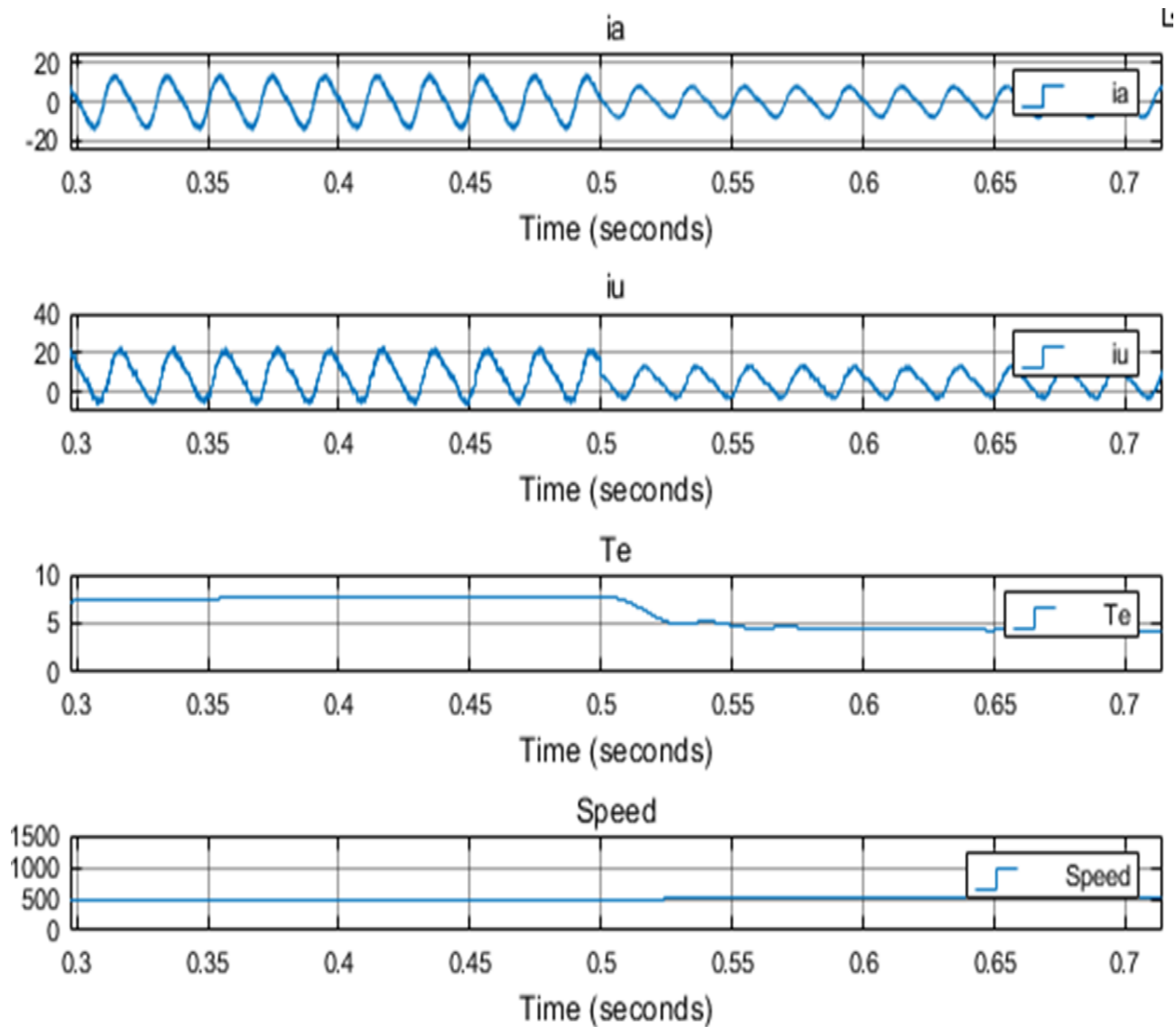


fig.6.15. Currents in phase A and U, speed, and output torque.

6.2.4.3 LOAD IS CONSTANT AND SPEED IS VARIABLE:

The load is changed at 0.5 amplitude

The phase currents I_a , I_u and speed changes also partial change in torque due to speed change

Reference speed=[500 250 250]

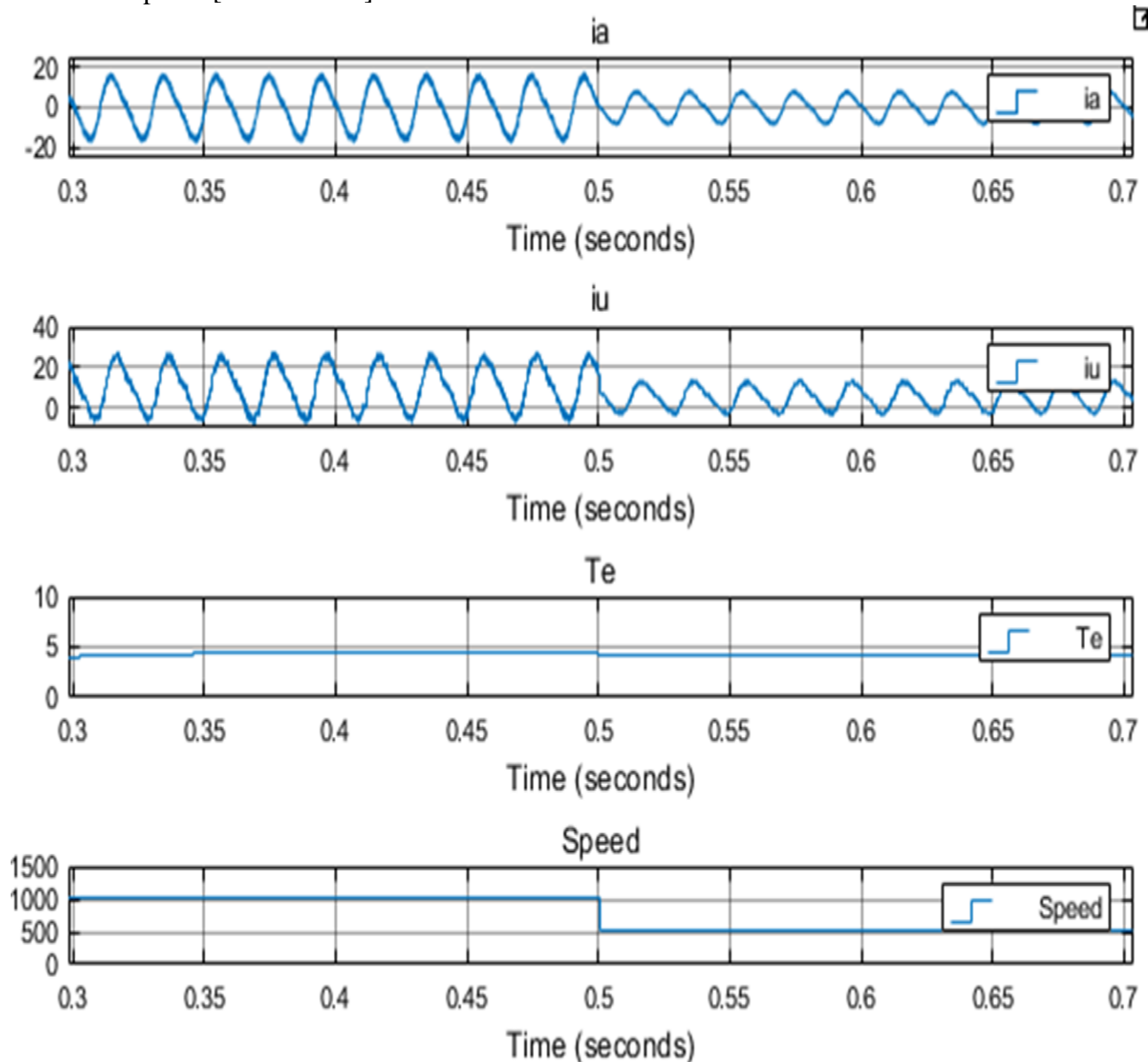


fig.6.16. Currents in phase A and U, speed, and output torque.

6.3 RESULTS ANALYSIS:

The project focuses on the integration of a reconstructed on-board charger with a six-phase machine for solar-powered electric vehicles (EVs). The analysis was conducted using MATLAB/Simulink 2018(a), examining two primary cases: DC charging mode and simultaneous charging and driving mode. In the DC charging mode, both steady-state and dynamic state analyses were performed for connections to a DC grid and a solar power source. The steady-state analysis revealed that the system achieved optimal voltage and current levels, with power output and efficiency metrics demonstrating favorable performance for both connection types. Wave form representations illustrated the differences in performance, highlighting the advantages of solar connection in terms of sustainability and reduced operational costs.

In the dynamic state analysis, the system's response to sudden changes in load or input conditions was evaluated. Time-domain plots showcased the transient behavior of voltage and current waveforms, indicating the system's ability to stabilize quickly after disturbances. This resilience is crucial for maintaining performance in real-world applications where load conditions can fluctuate.

The simultaneous charging and driving mode was analyzed under three distinct states. In the first state, where both load and speed were constant, the system demonstrated efficient power distribution between charging and driving, with metrics indicating high overall efficiency. The second state involved variable load while maintaining constant speed. This analysis revealed that as the load varied, the system effectively adapted, maintaining charging efficiency and driving performance. The third state, characterized by constant load and variable speed, highlighted the impact of speed changes on system performance. The results indicated that while the system could handle variations in speed, there were critical thresholds beyond which efficiency began to decline.

A comparative analysis of the results from the DC charging mode and the simultaneous charging and driving mode underscored the strengths and limitations of each approach. The DC charging mode provided stable performance under controlled conditions, while the simultaneous mode offered flexibility and adaptability in real-world scenarios. The findings suggest that the reconstructed on-board charger and six-phase machine hold significant potential for enhancing the performance of solar-powered electric vehicles.

CONCLUSION & FUTURE SCOPE

CONCLUSION:

In this project, a novel EDROC with the ability of simultaneous driving and charging operation for EV incorporating six-phase machines is proposed. The main contributions of this project over earlier works are concluded as follows. A novel EDROC topology circuit for EV with capabilities of simultaneous driving and charging, and dc charging is studied, in which supernumerary components are not required except for two mode switches. To ensure the safety operation in the simultaneous driving and charging mode, the working principles of symmetrical six-phase PMSM and its operation modes are analyzed in considerable detail. Thereafter, a reasonable control scheme is explored. To reduce machine phase current ripple and produce zero electromagnetic torque in dc charging mode, average duty strategy associated with the phase shift technique is incorporated in the EDROC system.

FUTURE SCOPE:

The Electric-Drive-Reconstructed Onboard Charger (EDROC) enhances solar-powered electric vehicles by enabling simultaneous driving and charging. Future developments include optimizing energy efficiency, integrating with smart grids, refining control strategies, assessing environmental impacts, and conducting real-world testing, ultimately promoting sustainable transportation and broadening market adoption of innovative electric vehicle technologies.

REFERENCES

- [1] Y. Zhang, J. Fang, F. Gao, S. Gao, D. Rogers, and X. Zhu, “Integrated high- and low-frequency current ripple suppressions in a single-phase onboard charger for EVs,” *IEEE Trans. Power Electron.*, vol. 36, no. 2, pp. 1717–1729, Feb. 2021.
- [2] D. Abeywardana, P. Acuna, and B. Hredzak, “Single-phase boost inverterbased electric vehicle charger with integrated vehicle to grid reactive power compensation,” *IEEE Trans. Power Electron.*, vol. 33, no. 4, pp. 3462–3471, Apr. 2018.
- [3] R. Hou and A. Emadi, “Applied integrated active filter auxiliary power module for electrified vehicles with single-phase onboard chargers,” *IEEE Trans. Power Electron.*, vol. 32, no. 3, pp. 1860–1871, Mar. 2017.
- [4] J. Gao, W. Sun, D. Jiang, Y. Zhang, and R. Qu, “Improved operation and control of single-phase integrated on-board charger system,” *IEEE Trans. Power Electron.*, vol. 36, no. 4, pp. 4752–4765, Apr. 2021.
- [5] S. Sharma, M. Aware, and A. Bhowate, “Integrated battery charger for EV by using three-phase induction motor stator windings as filter,” *IEEE Trans. Transport. Electrific.*, vol. 6, no. 1, pp. 83–94, Mar. 2020.
- [6] M. Tong, M. Cheng, and W. Hua, “A single-phase on-board two-stage integrated battery charger for EVs based on a five-phase hybrid-excitation flux-switching machine,” *IEEE Trans. Veh. Technol.*, vol. 69, no. 4, pp. 3793–3804, Apr. 2020.
- [7] S. Wang and P.W. Lehn, “A 3-phase electric vehicle charger integrated with dual inverter drive,” *IEEE Trans. Transport. Electrific.*, to be published, doi: 10.1109/TTE.2021.3102192.
- [8] H. Raherimihaja, Q. Zhang, and T. Na, “A three-phase integrated battery charger for EVs based on six-phase open-end winding machine,” *IEEE Trans. Power Electron.*, vol. 35, no. 11, pp. 12122–12132, Nov. 2020.
- [9] R. Shi, S. Semsar, and P. Lehn, “Constant current fast charging of electric vehicles via a DC grid using a dual-inverter drive,” *IEEE Trans. Ind. Electron.*, vol. 64, no. 9, pp. 6940–6949, Sep. 2017.
- [10] D. Woo, D. Joo, and B. Lee, “On the feasibility of integrated battery charger utilizing traction motor and inverter in plug-in hybrid electric vehicles,” *IEEE Trans. Power Electron.*, vol. 30, no. 12, pp. 7270–7281, Dec. 2015.
- [11] D. Kim, M. Kim, and B. Lee, “An integrated battery charger with high power density and efficiency for electric vehicles,” *IEEE Trans. Power Electron.*, vol. 32, no. 6, pp. 4553–4565, Jun. 2017.
- [12] X. Lu, K. Iyer, and K. Mukherjee, “Investigation of integrated charging and discharging incorporating interior permanent magnet machine with damper bars for electric vehicles,” *IEEE Trans. Energy Convers.*, vol. 31, no. 1, pp. 260–269, Mar. 2016.
- [13] Y. Zhang, J. Fang, and F. Gao, “Second-harmonic ripple voltage suppression of integrated single-phase pulse width modulation rectifier charging system for EVs,” *IEEE Trans. Power Electron.*, vol. 35, no. 4, pp. 3616–3626, Apr. 2020.

-
- [14] W. Lhomme, P. Delarue, and T. Moraes, “Integrated traction/charge/air compression supply using three-phase split-windings motor for electric vehicles,” *IEEE Trans. Power Electron.*, vol. 33, no. 11, pp. 10003–10012, Nov. 2018.
- [15] I. Subotic, N. Bodo, and E. Levi, “Integration of six-phase EV drivetrains into battery charging process with direct grid connection,” *IEEE Trans. Energy Convers.*, vol. 32, no. 3, pp. 1012–1022, Sep. 2017.
- [16] X. Liu, F. Yu, J. Mao, and H. Yang, “Pre- and post-fault operations of six-phase electric-drive-reconstructed onboard charger for electric vehicles,” *IEEE Trans. Transport. Electrific.*, to be published, doi: 10.1109/TTE.2021.3113316.
- [17] S. Ali, D. Mascarella, and G. Joos, “Torque cancelation of integrated battery charger based on six-phase permanent magnet synchronous motor drives for electric vehicles,” *IEEE Trans. Transport. Electrific.*, vol. 4, no. 2, pp. 344–354, Jun. 2018.
- [18] F. Yu, W. Zhang, and Y. Shen, “A nine-phase permanent magnet electricdrive-reconstructed onboard charger for electric vehicle,” *IEEE Trans. Energy Convers.*, vol. 33, no. 4, pp. 2091–2101, Dec. 2018.
- [19] G. Chandra Mouli, J. Schijffelen, and M. Heuvel, “A 10 kW solar-powered bidirectional EV charger compatible with chademo and COMBO,” *IEEE Trans. Power Electron.*, vol. 34, no. 2, pp. 1082–1098, Feb. 2019.
- [20] A. Singh, M. Badoni, and Y. Tatte, “A multifunctional solar PV and grid based on-board converter for electric vehicles,” *IEEE Trans. Veh. Technol.*, vol. 69, no. 4, pp. 37s17–3727, Apr. 2020.